



## OPEN Modeling monkeypox transmission with a compartmental framework to evaluate testing, isolation and public awareness strategies

Akindele Akano Onifade<sup>1,9</sup>, Oluwaseun Adenike Akindele<sup>2,9</sup>, Irfan Ahmad<sup>3,9</sup>, Muhammad Altaf Khan<sup>4,5,6,7,9</sup>✉, Nurulfiza Mat Isa<sup>5,9</sup> & Ebraheem Alzahrani<sup>8,9</sup>

Monkeypox (mpox), a viral infectious disease affecting both humans and non-human primates, has posed significant public health challenges, particularly in light of recent global outbreaks. This study develops a deterministic mathematical model to analyze the transmission dynamics of mpox, with a focus on the effects of self-isolation, testing, and public awareness in mitigating the spread of the virus. The model is calibrated using incidence data from the United States and employs a nonlinear least squares fitting method to reflect the observed epidemic trends accurately. The analysis identifies key parameters influencing the spread of mpox, including the transmission probabilities between human to human and mammal to human, as well as the effectiveness of public awareness campaigns. Stability analysis of the model reveals that the mpox-free equilibrium is locally asymptotically stable (LAS) when the basic reproduction number  $\mathcal{R}_0$  is less than 1, indicating disease elimination. Conversely, when  $\mathcal{R}_0 > 1$ , the presence of a stable endemic equilibrium suggests the potential for sustained transmission if control measures are not adequately implemented. Sensitivity analysis reveals that factors like transmission rates, public awareness levels, and isolation rates significantly impact the disease's spread, providing insights into which interventions may be most effective. Numerical simulations demonstrate the potential of targeted strategies, showing that even partial adherence to isolation and public awareness strategies can significantly reduce new infections. A comprehensive approach combining effective isolation, expanded testing, and targeted awareness campaigns is crucial in managing mpox outbreaks. This approach provides valuable guidance for public health strategies, supporting the design of interventions that can prevent the spread of mpox and ensure better preparedness for future outbreaks.

Emerging and re-emerging infectious diseases continue to pose significant global health threats. Their spread is often driven by zoonotic spillovers, environmental changes, and increased global travel. Non-pharmaceutical interventions such as isolation, testing, and public health awareness have become crucial tools for managing outbreaks, especially where pharmaceutical options are limited or unavailable. Mathematical modeling plays a vital role in understanding transmission dynamics, forecasting outbreaks, and evaluating control strategies.

Mpox, sometimes known as monkeypox, stands as a significant health challenge in tropical and subtropical regions, spurred by viral infections from the mpox virus<sup>1,2</sup>. These viruses manifest in two primary forms: the Clade I strain and the Clade II strain. The mpox Clade I strain is found in Central Africa, while the Clade II strain is typically found in West African countries<sup>3</sup>. The mpox Clade I strain has been identified as the most pathogenic (deadliest) virus with a substantially higher mortality rate compared to the Clade II strain<sup>3</sup>. Research

<sup>1</sup>Department of Computer Science and Mathematics, Mountain Top University, Ibafo, Nigeria. <sup>2</sup>Department of Chemistry, University of Ibadan, Ibadan, Nigeria. <sup>3</sup>Department of Clinical Laboratory Sciences, College of Applied Medical Science, King Khalid University, Abha 61421, Saudi Arabia. <sup>4</sup>Department of Mathematics, Saveetha School of Engineering, SIMATS, Saveetha University, Chennai 602105, Tamil Nadu, India. <sup>5</sup>Laboratory of Vaccine and Biomolecules, Institute of Bioscience, Universiti Putra Malaysia, UPM, Serdang 43400, Selangor, Malaysia. <sup>6</sup>School of Health and Environmental Science, Korea University, Seoul 02841, South Korea. <sup>7</sup>Faculty of Natural and Agricultural Sciences, University of the Free State, Bloemfontein 9300, South Africa. <sup>8</sup>Department of Mathematics, Faculty of Science, King Abdulaziz University, Jeddah, Saudi Arabia. <sup>9</sup>Akindele Akano Onifade, Oluwaseun Adenike Akindele, Irfan Ahmad, Altaf Khan, Nurulfiza Mat Isa, Ebraheem Alzahrani contributed equally to this work. ✉email: [altafkhan@upm.edu.my](mailto:altafkhan@upm.edu.my); [muhammadaltafkhan@korea.ac.kr](mailto:muhammadaltafkhan@korea.ac.kr)

on animals has also shown that Clade I strain pathogenicity is of greater significance compared to Clade II pathogenicity<sup>3</sup>. This seems to be particularly true for the Clade IIb strain, the virus responsible for the 2022–2023 global epidemic, to which the disease was typically not fatal.

The mpox Clade IIb strain outbreak started in 2022 and continues to this day worldwide, especially in many African countries. In the Democratic Republic of the Congo (DRC) and many other African nations, there are escalating mpox outbreaks of Clades Ia and Ib<sup>1,2,4</sup>. In August 2024, the Clade Ib strain was identified outside Africa<sup>5</sup>. Small mammals (e.g., squirrels, monkeys, etc) are susceptible to mpox; however, the virus's natural reservoir host remains unclear to this day<sup>1,2,4</sup>. The prevalence of mpox has been propagating worldwide since spring 2022, especially on continents other than Africa, where outbreaks had formerly been scarce. Global prevalence statistics paint a grim picture, with an estimated 100,000 individuals affected worldwide<sup>5</sup>. Based on the information released by the Africa Centers for Disease Control and Prevention<sup>3,6</sup>, mpox Clade I variant cases in 2024 have been alarmingly spiked<sup>3</sup>. This continues with the trend of increasing rates first identified in 2023. Mpox cases or incidence rose by 160 % in 2024 compared to last year (2023), same time<sup>3</sup>, while fatalities rose by 195 percent<sup>5</sup>. The DRC prevalence statistics paint a grim picture, with an estimated 17,794 confirmed cases in 2024, with 535 deaths<sup>5</sup>. The CDC highlights the gravity of the situation, revealing a staggering 66% of Clade I strain prevalence rate and an 82% mpox-related death rate among children % in African countries<sup>5</sup>. However, it remains unclear whether these deaths are caused by mpox Clade Ib strain or the earlier Clade I strain<sup>5</sup>.

Person-to-person transmission of mpox is primarily via intimate contact with a person infected with the mpox virus, particularly family members<sup>1,2,4,7</sup>. Intimate contact or relationships, for example, kissing, intercourse, or touching an infected person, can result in transmission of the infection<sup>1,7</sup>. People who have many sexual partners are most susceptible to contracting mpox<sup>1,2,4,8</sup>. Mpox can still be transmissible from person to person until lesions have healed and new skin is formed<sup>1</sup>. A few people may become infected without showing any signs of infection with the mpox virus. Nevertheless, contracting the mpox virus from a person who does not show any sign of having mpox has not been reported or documented<sup>1,2,4</sup>. People who have underlying infections, humans with a low immune system, children, and pregnant people are most susceptible to mpox infection<sup>1,2,4</sup>.

Detecting the mpox virus by utilizing PCR is the preferred laboratory test for mpox<sup>1</sup>. Taking a blood sample from a suspected human for testing is not recommended<sup>1</sup>. However, swabs of the anus or throat are suggested for testing for the mpox virus in human, especially when there are no skin lesions<sup>1</sup>. Differentiating mpox from similar infections such as chickenpox, measles, bacterial skin infections, and other sexually transmitted infections is essential<sup>1,7,8</sup>. Infectious humans with the mpox virus may also have another sexually transmitted illness<sup>1</sup>. Also, a child infected with mpox may have chickenpox; therefore, proper tests must be conducted to know whether the child has mpox or chickenpox or both infections<sup>1</sup>.

Detection of exposed individuals at the early stage of infection and providing supportive treatment are critical in disease management and preventing potential spread. Non-pharmaceutical therapies, for example, vaccination, self-isolation, public awareness, and early testing, help mitigate the spread of mpox in the community<sup>1,7</sup>. Reducing rash and pain when treating mpox infection is another primary objective in managing the disease<sup>7</sup>. Presently, no effective antiviral drug has been discovered or developed for the treatment of mpox infection<sup>1,7</sup>.

Mathematical modeling has become a powerful tool for understanding infectious disease spread and guiding public health responses. Previous studies have successfully applied modeling approaches to mpox transmission, revealing key insights about its dynamics and control<sup>9–14</sup>. However, most existing models share two important limitations: their primary focus on studying African endemic regions, and analyzing interventions such as isolation or testing, rather than examining the combined effects of isolation, testing, and awareness using real data. Moreover, mathematical modeling is a significant instrument for comprehending the transmission dynamics of illness, making decisions on methods of intervention, and mitigating diseases<sup>15–17</sup>. Given this context, numerous deterministic models, in the form of ordinary differential equations, have been used to examine mpox transmission dynamics and control measures aimed at reducing infection<sup>9–14</sup>. We refer readers to the aforementioned citations for a comprehensive understanding of previous efforts to combat mpox infection using mathematical models. Despite efforts in recent years focusing on preventive strategies, the persistence and pervasiveness of mpox underscore the need for a comprehensive approach. Public decision on people's willingness to follow government-implemented control measures, a critical yet often overlooked factor in disease transmission dynamics, necessitates closer scrutiny<sup>18</sup>. While anecdotal evidence highlights the role of public compliance in disease spread, systematic investigations into its nuances and impact remain limited. The dynamic deterministic model stands as a stalwart mathematical framework, meticulously crafted for dissecting agent decisions and strategic maneuvers within dynamic environments. This model delves into the intricate dynamics of decision-making, carefully considering the ripple effects across the overarching system. Through the art of simulating diverse scenarios and scrutinizing equilibrium solutions, dynamic deterministic models yield profound insights into optimal strategies, system dynamics, and the far-reaching implications of varying decision-making paradigms in complex systems over temporal horizons. In a recent work, the author focused on studying the mpox disease dynamics under the cases reported in the African region. The model is formulated and provides results regarding the disease control in Africa. The authors in<sup>19</sup> used the non-integer modeling approach to study the dynamics of mpox. They presented results offering reasonable insights into the control of mpox. Different approaches were considered in<sup>20</sup> to study and understand the mpox disease dynamics. Four different epidemic models for the dynamics of the mpox disease outbreaks have been considered in<sup>21</sup>. Governmental interventions on mpox disease dynamics were investigated in<sup>22</sup>. A mathematical approach to study mpox infection in regions where HIV is endemic was considered in<sup>23</sup>. The impact of various infection routes to understand mpox transmission dynamics was analyzed in<sup>24</sup>.

In the United States, there have been no reported cases of Clade I mpox, while Clade II continues to circulate at low levels. Concerns about the risk of mpox in children have arisen, especially since many cases in regions

with regular outbreaks involve children. In endemic areas of western and central Africa, children often contract mpox through contact with wild animals that act as a reservoirs of the virus, which can then spread to humans and subsequently to close contacts. However, animals in U. S. do not carry the mpox virus. The high number of pediatric cases in the current DRC outbreak likely results from household transmission, driven by many factors such as crowded living conditions and poor sanitation. In contrast, the U. S. has a lower risk of similar spread due to differences in household structures, access to disinfectants, and improved medical care. CDC simulations of Clade I mpox transmission through close contact within and between households, including scenarios involving children, suggest that such transmission would not likely lead to a significant number of cases in the U. S.

The information about the mpox cases in the United States in 2024, including the rise to 656 cases by March 30 and the focus on vaccination efforts, is drawn from reports and experts' commentary on the trends and responses to the outbreak. The analysis highlights that despite the increase in cases, the situation is less severe than the 2022 outbreak, with states like New York and California experiencing a higher number of infections<sup>25</sup>. Additionally, discussions on the factors influencing the uptick in cases and vaccination efforts can be found therein<sup>25</sup>.

While significant modeling efforts have been devoted to mpox transmission dynamics (see the literature mentioned above), critical gaps remain in understanding how combined interventions such as testing, isolation, and awareness interact to influence disease spread, particularly in non-endemic areas such as the United States, under real reported cases. The existing literature has missed how awareness campaigns enhance testing uptake or how testing availability could influence isolation compliance. Our study addresses this gap by developing and analyzing a novel, comprehensive compartmental mathematical model under real data that uniquely integrates these strategies. A review of the existing literature reveals that no prior work has applied mathematical modeling to investigate mpox dynamics in the simultaneous presence of isolation, testing, and awareness, especially with real data. Unlike prior studies<sup>9,10,14</sup>, which often consider these interventions in isolation or assume idealized conditions, our model uniquely integrates a behavioral feedback mechanism. To be more specific, it captures how public perceptions shaped through awareness modulate the effectiveness of interventions, thereby influencing individual compliance with testing and isolation guidelines. This advances the research on mpox in several ways: incorporating behavioral response, real data calibration, and the combined impacts of isolation, testing and awareness; capturing how public perceptions influences efficacy; addressing a critical gap in region specific contexts where the disease is non-endemic; and unifying the effects, isolation, testing, and awareness campaigns, making a novel contribution to the field and mpox public policy design.

## Materials and methods

### Model development

In this study, the mpox model is constructed using ordinary differential equations (ODEs) to quantify the influence of self-isolation, testing for the mpox virus, and awareness in mitigating the illness. The study targeted two different populations that represent the transmission of the mpox virus in humans (hosts) and mammals. The human population is categorized into five classes: susceptible humans  $S_h(t)$ , exposed humans  $E_h(t)$ , infected humans  $I_h(t)$ , self-isolated humans  $S_{fih}$ , and recovered humans  $R_h(t)$ . Humans are recruited into the susceptible class,  $S_h$ , through birth at a rate  $\Lambda_h$ . They can become infected with either the Clade I or Clade II strain, with the force of infection given by

$$\lambda_h = \frac{\beta_{ah}I_a}{N_h} + \frac{\beta_h I_h}{N_h}, \quad (1)$$

where  $\lambda_h$  represents the combined transmission rate from infected animals and humans,  $\beta_{ah}$  denotes the probability that contact with an infected mammal results in human infection, while  $\beta_h$  represents the probability that contact with an infected human leads to infection.  $I_a$  is the density of mammals infected with the mpox virus,  $I_h$  is the density of infected humans, and  $N_h$  is the total human population. To reduce the disease transmission, we assume that a proportion  $\theta$  of susceptible humans are aware of the disease and take precautions to protect themselves. The remaining proportion who are unaware of the disease move to the exposed class upon contact with an infectious individual. Those who are already aware of the disease remain vigilant by taking precautions to avoid contact with mpox.  $0 \leq \theta \leq 1$  is the efficacy of being vigilant. Exposed individuals are latently infected, meaning they have no symptoms and are not yet contagious. These individuals progress to the infectious stage at a rate  $\alpha_h$ , where  $\alpha_h^{-1}$  represents the average incubation period. The parameter  $\tau$  denotes the time taken to trace and test exposed humans before they enter self-isolation. A fraction  $x$  of exposed individuals who test positive for the mpox virus (either Clade I or II) are willing or agree to self-isolate, and thus transition to the self-isolated class. Similarly, a fraction  $\kappa$  of infected individuals voluntarily adopt self-isolation (i.e., home self-isolation), and also move to the self-isolated class. Although some people find it difficult to self-isolate because of their jobs. The parameter  $\rho$  represents the detection rate of exposed humans who join the self-isolated class, and  $q$  represents the isolation rate. Humans die with a natural mortality rate  $\mu_h$ , while their disease-induced mortality rate is  $\delta_h$ . The recovery rate of infected humans and self-isolated humans is respectively given by  $r$  and  $\gamma_s$ . The loss of immunity of recovered people is given by the rate  $\omega$ .

We assume that mammals are born susceptible into the susceptible class at a rate  $\Lambda_a$ . They become exposed to the mpox virus at a rate of infection given by:

$$\lambda_a = \frac{\beta_2 I_h}{N_h} + \frac{\beta_a I_a}{N_a}, \quad (2)$$

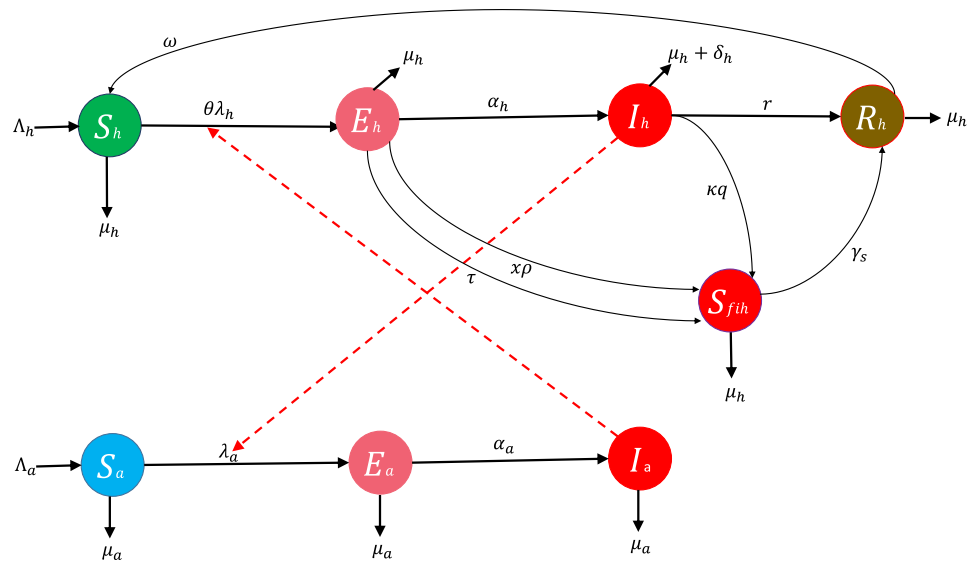


**Fig. 1.** Flow diagram illustrating the transmission dynamics of the mpox model, incorporating key factors such as self-isolation in the human compartment, testing for the mpox virus, and public awareness measures.

Symbol	Description
$\Lambda_h$	Birth rate of humans
$\mu_h$	Human natural mortality
$\Lambda_a$	Birth rate of mammals
$\mu_a$	Mammal natural mortality
$\beta_{ah}$	probability that a contact by an infected mammal will result in an infection
$\beta_2$	Transmission probability of mpox virus from humans to animals
$\beta_a$	Transmission probability of mpox virus from animals to animals
$\beta_h$	probability that a contact by an infected human will result in an infection
$\rho$	Detection rate (rate at which individuals become tested)
$q$	Isolation rate of infectious humans
$x$	A portion of patients tested positive for the Mpox virus
$\kappa$	Fraction of infectious humans that adopt self-isolation
$\alpha_h^{-1}$	Duration of the incubation period in humans
$\theta$	Efficacy of being vigilant about the infection
$\tau$	time taken to trace and test exposed humans before self-isolation
$\omega$	Natural immunity waning rate
$r$	Recovery rate of non-isolated infectious humans
$\gamma_s$	Recovery rate of isolated infectious humans
$\delta_h$	Humans disease-induced mortality
$\alpha_a^{-1}$	Duration of the incubation period in mammals

**Table 1.** Details of the parameters and their numerical value.

where  $\beta_2$  represents the transmission among infected humans and susceptible mammals, and  $\beta_a$  is the transmission rate among infected mammals and susceptible mammals. The population of mammals is classified into three groups, that is, the susceptible, exposed, and the infected, shown respectively by  $S_a(t)$ ,  $E_a(t)$ , and  $I_a(t)$ . Mammals die with a natural mortality rate  $\mu_a$ . The exposed mammal population progresses to the infectious mammal class at a rate  $\alpha_a$  after the incubation period. Based on the aforementioned description of the mpox model, we present eight-dimensional nonlinear ODEs, and the transition diagram is shown in Fig. 1 to explain the transmission dynamics of mpox infection. The definition of the mpox model parameters is given in Table 1. We assume that each individual in the population is mixed homogeneously. Although demographic processes such as birth and death rates are considered, the populations of mammals and humans are assumed to be constant during the mpox outbreak. There is no permanent recovery, and hence recovered individuals may lose their immunity and become reinfected.

$$\begin{aligned}
 \dot{S}_h &= \Lambda_h - \theta\lambda_h S_h + \omega R_h - \mu_h S_h, \\
 \dot{E}_h &= \theta\lambda_h S_h - x\rho E_h - (\alpha_h + \tau + \mu_h)E_h \\
 \dot{I}_h &= \alpha_h E_h - \kappa q I_h - (r + \delta_h + \mu_h)I_h, \\
 \dot{S}_{fih} &= (x\rho + \tau)E_h + \kappa q I_h - (\gamma_s + \mu_h)S_{fih}, \\
 \dot{R}_h &= \gamma_s S_{fih} + r I_h - (\omega + \mu_h)R_h, \\
 \dot{S}_a &= \Lambda_a - \lambda_a S_a - \mu_a S_a, \\
 \dot{E}_a &= \lambda_a S_a - (\alpha_a + \mu_a)E_a, \\
 \dot{I}_a &= \alpha_a E_a - \mu_a I_a.
 \end{aligned}
 \tag{3}$$

### Mpox model invariant region and boundedness

In this part, we discuss the essential elements of the proposed model. Evaluating the total human population, we get  $N_h(t) = S_h(t) + E_h(t) + I_h(t) + S_{fih}(t) + R_h(t)$ . The derivative of the expression gives  $\frac{dN_h}{dt} = \Lambda_h - \delta_h I_h(t) - \mu_h N_h(t)$ . This implies that  $\frac{dN_h}{dt} \leq \Lambda_h - \mu_h N_h(t)$ . Evaluating this inequality, we obtain

$$N_h \leq \frac{\Lambda_h}{\mu_h} + \left( N_h(0) - \frac{\Lambda_h}{\mu_h} \right) e^{-\mu_h t}.$$

Utilizing a similar approach for the animal population, we obtain  $N_a = S_a(t) + E_a(t) + I_a(t)$ . The derivative of the expression gives  $\frac{dN_a}{dt} = \Lambda_a - \mu_h N_h(t)$ . Evaluating this expression, we have

$$N_a \leq \frac{\Lambda_a}{\mu_a} + \left( N_a(0) - \frac{\Lambda_a}{\mu_a} \right) e^{-\mu_a t}.$$

As  $t \rightarrow \infty$ , we obtain  $N_h(t) \leq \frac{\Lambda_h}{\mu_h}$  and  $N_a(t) \leq \frac{\Lambda_a}{\mu_a}$ . Thus, whenever  $t \geq 0$ , the mpox model (3) has non-negative components or variables. It can be concluded that the mpox model (3) is epidemiologically well-posed and of biological interest to study the dynamical parts in feasible region, which is obtained as  $\Psi = \Psi_h \times \Psi_a \subseteq \mathfrak{R}_+^5$ , where  $\Psi_h = \varepsilon_1 \in \mathfrak{R}_+^5 : \varepsilon_2 \leq \frac{\Lambda_h}{\mu_h}$  and  $\Psi_a = \varepsilon_3 \in \mathfrak{R}_+^3 : \varepsilon_4 \leq \frac{\Lambda_a}{\mu_a}$ , where  $\varepsilon_1 = (S_h, E_h, I_h, S_{fih}, R_h), \varepsilon_2 = S_h + E_h + I_h + S_{fih} + R_h, \varepsilon_3 = S_a, E_a, I_a$  and  $\varepsilon_4 = S_a + E_a + I_a$ .

Next, we shall utilize the theorem below to prove the positivity and boundedness of the mpox model (3) solution.

*Theorem 1* Suppose the starting values of the mpox model components or variables at  $t = 0$  are positive, that is  $S_h(0) > 0, E_h(0) > 0, I_h(0) > 0, S_{fih}(0) > 0, R_h(0) > 0, S_a(0) > 0, E_a(0) > 0, I_a(0) > 0$ , then whenever  $t > 0$  the mpox model-relation solution will be non-negative  $\forall t > 0$ .

*Proof* To prove the above theorem, we take the first equation in (3)

$$\dot{S}_h = \Lambda_h - (\theta\lambda_h + \mu_h)S_h + \omega R_h \geq \Lambda_h - (\theta\lambda_h + \mu_h)S_h.$$

It can be written as

$$\dot{S}_h + (\theta\lambda_h + \mu_h)S_h \geq \Lambda_h.$$

Using integration, we get

$$\frac{d}{dt} \left[ S_h(t) \exp\{\mu_h t + \theta \int_0^t \lambda_h(s) ds\} \right] \geq \Lambda_h \left[ \exp\{\mu_h t + \theta \int_0^t \lambda_h(s) ds\} \right].$$

Simplifying further, we obtain

$$\begin{aligned}
 S_h(t) &\geq S_h(0) \left[ \exp\{-\mu_h t - \theta \int_0^t \lambda_h(s) ds\} \right] + \left[ \exp\{-\mu_h t - \theta \int_0^t \lambda_h(s) ds\} \right] \\
 &\quad \times \int_0^t \Lambda_h \left[ \exp\{\mu_h y + \theta \int_0^y \lambda_h(y) dy\} \right] dy > 0.
 \end{aligned}$$

where  $S_h^0$  denotes the starting value before the epidemic, and it is positive. So,  $S_h > 0$ . Utilizing the same approach as above to prove the other mpox equations in (3), it can be shown that  $E_h \geq 0, I_h \geq 0, S_{fih} \geq 0, R_h \geq 0, S_a \geq 0, E_a \geq 0, I_a \geq 0 \forall t > 0$ . The positive solution presented in the aforementioned theorem is bounded. □

### Equilibria and threshold quantity ( $\mathcal{R}_0$ )

Mpox free equilibrium (MFE) of the model (3) can be represented by  $D_0$ , which is given by

$$D_0 = (S_h^0, 0, 0, 0, 0, S_a^0, 0, 0) = \left( \frac{\Lambda_h}{\mu_h}, 0, 0, 0, 0, \frac{\Lambda_a}{\mu_a}, 0, 0 \right). \tag{4}$$

Next, we calculate the basic threshold quantity or parameter, represented by  $\mathcal{R}_0$ , by utilizing the next-generation technique, which is explained briefly in<sup>26</sup>. Following this method, we have

$$F = \begin{pmatrix} 0 & \theta\beta_h & 0 & \theta\beta_{ah} \\ 0 & 0 & 0 & 0 \\ 0 & \frac{\beta_2 S_a^0}{S_h^0} & 0 & \beta_a \\ 0 & 0 & 0 & 0 \end{pmatrix}, \quad V = \begin{pmatrix} \Phi_1 & 0 & 0 & 0 \\ -\alpha_h & \Phi_2 & 0 & 0 \\ 0 & 0 & \Phi_5 & 0 \\ 0 & 0 & -\alpha_a & \mu_a \end{pmatrix}.$$

The dominant eigenvalue  $\rho(FV^{-1})$  provides the basic threshold quantity or parameter, which can be obtained as follows:

$$\mathcal{R}_0 = \frac{\mathcal{R}_1 + \sqrt{\mathcal{R}_1^2 + 4\mathcal{R}_2}}{2}, \tag{5}$$

where

$$\begin{aligned} \mathcal{R}_1 &= \frac{\Phi_1 \Phi_2 \alpha_a \beta_a + \Phi_5 \theta \mu_a \alpha_h \beta_h}{\Phi_1 \Phi_2 \Phi_5 \mu_a}, \\ &= \frac{\alpha_a \beta_a}{\Phi_5 \mu_a} + \frac{\theta \alpha_h \beta_h}{\Phi_1 \Phi_2}, \\ &= \mathcal{R}_1^1 + \mathcal{R}_1^2, \end{aligned}$$

and

$$\mathcal{R}_2 = \frac{\theta \alpha_a \alpha_h (\beta_2 S_a^0 \beta_{ah} - \beta_a \beta_h S_h^0)}{\Phi_1 \Phi_2 \Phi_5 \mu_a S_h^0}.$$

where  $\Phi_1 = \alpha_h + \mu_h + \tau + \rho x$ ,  $\Phi_2 = \delta_h + \mu_h + \kappa q + r$ ,  $\Phi_3 = \gamma_s + \mu_h$ ,  $\Phi_4 = \omega + \mu_h$ ,  $\Phi_5 = \alpha_a + \mu_a$ . Here,  $\mathcal{R}_1$  represents the sub-basic reproduction number that contributes to the new infections from humans to humans, and from animals to humans, animals to humans, animals to animals, and from humans to animals. The sub-basic reproduction number  $\mathcal{R}_2$  measures the contribution from animals to humans, humans to humans, animals to humans, and from humans to animals.

Next, we present the theorem below to demonstrate that the mpox model (3) is locally asymptotically stable.

### Locally stable of mpox free equilibrium

**Theorem 2** *The Mpox-free infection equilibrium  $D_0$  is locally stable (asymptotically stable) if  $\mathcal{R}_0 < 1$ , and unstable otherwise.*

*Proof* The Jacobian matrix is evaluated at the mpox-free equilibrium  $D_0$ ,

$$J(D_0) = \begin{pmatrix} -\mu_h & 0 & -\theta\beta_h & 0 & \omega & 0 & 0 & -\theta\beta_{ah} \\ 0 & -\Phi_1 & \theta\beta_h & 0 & 0 & 0 & 0 & \theta\beta_{ah} \\ 0 & \alpha_h & -\Phi_2 & 0 & 0 & 0 & 0 & 0 \\ 0 & x\rho + \tau & \kappa q & -\Phi_3 & 0 & 0 & 0 & 0 \\ 0 & 0 & r & \gamma_s & -\Phi_4 & 0 & 0 & 0 \\ 0 & 0 & -\frac{\beta_2 S_a^0}{S_h^0} & 0 & 0 & -\mu_a & 0 & -\beta_a \\ 0 & 0 & \frac{\beta_2 S_a^0}{S_h^0} & 0 & 0 & 0 & -\Phi_5 & \beta_a \\ 0 & 0 & 0 & 0 & 0 & 0 & \alpha_a & -\mu_a \end{pmatrix},$$

where  $\Phi_1 = \alpha_h + \mu_h + \tau + \rho x$ ,  $\Phi_2 = \delta_h + \mu_h + \kappa q + r$ ,  $\Phi_3 = \gamma_s + \mu_h$ ,  $\Phi_4 = \omega + \mu_h$ ,  $\Phi_5 = \alpha_a + \mu_a$ . The eigenvalues of the matrix  $J(D_0)$  with negative real parts are  $-\mu_h$ ,  $-\mu_a$ ,  $-(\omega + \mu_h)$  and  $-(\gamma_s + \mu_h)$ . The next four eigenvalues are calculated using the characteristic equation:

$$c_4 \lambda^4 + c_3 \lambda^3 + c_2 \lambda^2 + c_1 \lambda + c_0 = 0. \tag{6}$$

where

$$\begin{aligned}
 c_4 &= 1, \\
 c_3 &= \Phi_1 + \Phi_2 + \Phi_5 + \mu_a, \\
 c_2 &= \Phi_5 \mu_a (1 - \mathcal{R}_1^1) + (\Phi_1 + \Phi_2) (\mu_a + \Phi_5) + \Phi_1 \Phi_2 (1 - \mathcal{R}_1^2), \\
 c_1 &= (\Phi_1 + \Phi_2) \Phi_5 \mu_a (1 - \mathcal{R}_1^1) + \Phi_2 \Phi_1 (\mu_a + \Phi_5) (1 - \mathcal{R}_1^2), \\
 c_0 &= \mu_a \Phi_1 \Phi_2 \Phi_5 S_h^0 (1 - \mathcal{R}_1 - \mathcal{R}_2).
 \end{aligned}
 \tag{7}$$

It is obvious from Eq. (7) that the coefficients  $c_4$  and  $c_3$  are positive. To demonstrate the stability of equation (6), it is necessary to show that the coefficients  $c_i$  where  $i = 0, 1, 2$ , are also positive. While  $c_3$  and  $c_4$  are greater than zero,  $c_i$ , where  $i = 0, 1, 2$  can only be positive if  $\mathcal{R}_0 < 1$ . Furthermore, to investigate whether the coefficients  $c_i$  are positive, the Routh-Hurwitz criteria must be satisfied to ensure the eigenvalues have negative real parts. Hence, for Eq. (6), it is enough to show that the condition  $\mathcal{G} = c_3 c_1 c_2 > c_1^2 + c_3^2 c_0$  holds. This condition is readily satisfied, implying that the polynomial Eq. (6) yields eigenvalues with negative real parts. So, whenever  $\mathcal{R}_0 < 1$ , the mpox model (3) is locally asymptotically stable at the mpox-free equilibrium  $D_0$ . □

### Mpox model local stability of endemic equilibria

We present an analytical formulation for the endemic equilibrium and evaluate the possibility of a unique endemic equilibrium (EE). We represent the EE of the mpox model (3) by  $D_1$ , which is supplied by the values  $(S_h^*, E_h^*, I_h^*, Q_h^*, R_h^*, S_a^*, E_a^*, I_a^*)$ , and derive the required result as follows:

$$\begin{aligned}
 S_h^* &= \frac{\Lambda_h + \omega R_h^*}{\theta \lambda_h^* + \mu_h}, \\
 E_h^* &= \frac{\theta \lambda_h^* S_h^*}{x \rho + \alpha_h + \tau + \mu_h}, \\
 I_h^* &= \frac{\alpha_h E_h^*}{\kappa q + r + \delta_h + \mu_h}, \\
 S_{fih}^* &= \frac{(x \rho + \tau) E_h^* + \kappa q I_h^*}{\gamma_s + \mu_h}, \\
 R_h^* &= \frac{\gamma_s S_{fih}^* + r I_h^*}{\omega + \mu_h}, \\
 S_a^* &= \frac{\lambda_a}{\lambda_a^* + \mu_a}, \\
 E_a^* &= \frac{\lambda_h^* S_a^*}{\alpha_a + \mu_a}, \\
 I_a^* &= \frac{\alpha_a E_a^*}{\mu_a}.
 \end{aligned}
 \tag{8}$$

Utilizing Eq. (8) into  $\lambda_h^* = \frac{\beta_{ah} I_a^*}{N_h^*} + \frac{\beta_h I_h^*}{N_h^*}$ , and  $\lambda_a^* = \frac{\beta_2 I_h^*}{N_h^*} + \frac{\beta_a I_a^*}{N_a^*}$ . We first solve the result for  $\lambda_a^*$ , and then obtain the expression for  $\lambda_h^*$ . The result of  $\lambda_h^*$  is substituted back into the equation for  $\lambda_a^* = \frac{\beta_2 I_h^*}{N_h^*} + \frac{\beta_a I_a^*}{N_a^*}$ , and some rigorous calculations, we arrive at the following result:

$$k_1 \lambda_a^{*4} + k_2 \lambda_a^{*3} + k_3 \lambda_a^{*2} + k_4 \lambda_a^* + k_5 = 0
 \tag{9}$$

where,

$$\begin{aligned}
 k_1 &= \theta^2 \Phi_1 \Phi_2 \Phi_3^2 \Phi_4^2 \Phi_5^2 \alpha_h (\Phi_9 \alpha_h + \Phi_2 (\Phi_4 (\mu_h + \Phi_6) + (\Phi_4 + \Phi_6) \gamma_s)) (\alpha_a (\Lambda_a \beta_{ah} \delta_h + \mu_a \beta_h \Lambda_h) + \mu_a^2 \beta_h \Lambda_h), \\
 k_2 &= \Phi_2 (\Phi_{22} \alpha_a \Lambda_a \beta_{ah} + \Phi_5 \mu_a \Lambda_h (\Phi_7 \Phi_{18} \mu_a - 2 \theta \Phi_6 \Phi_7 \Phi_8 (\gamma_s + \Phi_4) + \Phi_{21})) \\
 &\quad + \theta \alpha_h (r \Phi_3 (\Phi_8 \Phi_{12} + \Phi_7 \Phi_{13}) \omega \alpha_a \Lambda_a \beta_{ah} + \kappa q \Phi_{16} \gamma_s + \Phi_{20}), \\
 k_3 &= \Phi_2 (\alpha_a \Lambda_a \beta_{ah} (\theta \Phi_6 (\Phi_7 \Phi_{14} - \Phi_8 \Phi_{13}) \omega \gamma_s + \Phi_1 \Phi_3 \Phi_4 \Phi_{28}) + \Phi_5 \Phi_{26} \mu_a \Lambda_h) \\
 &\quad + \theta \alpha_h (r \Phi_3 (\Phi_7 \Phi_{14} - \Phi_8 \Phi_{13}) \omega \alpha_a \Lambda_a \beta_{ah} + \Phi_5 \Phi_{27} \mu_a \Lambda_h + \kappa q \Phi_{23} \gamma_s), \\
 k_4 &= \Phi_5 \Phi_8 \mu_a^2 \Lambda_h (\Phi_3 \Phi_4 \Phi_{13} (\theta \alpha_h \beta_h - \Phi_1 \Phi_2) + \theta \Phi_8 \Phi_{29}) - \Phi_{14} (\theta \alpha_h (\Phi_8 \omega \alpha_a \Lambda_a \beta_{ah} (\kappa q \gamma_s + r \Phi_3) + \Phi_{31}) + \Phi_2 \Phi_{32}), \\
 k_5 &= \Phi_1 \Phi_2 \Phi_5 \mu_a^2 \Lambda_h (1 - \mathcal{R}_1 - \mathcal{R}_2).
 \end{aligned}
 \tag{10}$$

where  $\Phi_6 = \tau + \rho x$ ,

$$\begin{aligned}
 \Phi_7 &= \Phi_5 \Phi_1 \Phi_2 \Phi_3 \Phi_4, \quad \Phi_8 = \Phi_1 \Phi_2 \Phi_3 \Phi_4 (\alpha_a \beta_a - \Phi_5 \mu_a), \quad \Phi_9 = \kappa q \Phi_4 + \kappa q \gamma_s + \Phi_3 (r + \Phi_4), \\
 \Phi_{10} &= \Phi_6 (\gamma_s + \Phi_4) + \Phi_3 \Phi_4, \quad \Phi_{11} = \theta \alpha_a \alpha_h (\Phi_9 \beta_a + \beta_2 \Phi_3 \Phi_4), \quad \Phi_{12} = \theta \Phi_5 (\Phi_9 \alpha_h + \Phi_2 \Phi_{10}), \\
 \Phi_{13} &= \theta \Phi_2 \Phi_{10} (\alpha_a \beta_a - \Phi_5 \mu_a) + \theta \mu_a (\beta_2 \Phi_3 \Phi_4 - \Phi_5 \Phi_9) \alpha_h + \Phi_{11}, \\
 \Phi_{14} &= \beta_2 \theta \Phi_3 \Phi_4 \Phi_5 \mu_a \alpha_h, \quad \Phi_{15} = \Phi_4 \Phi_8 \Phi_{12} \beta_h + \Phi_7 (\Phi_4 \Phi_{13} \beta_h + 2 \Phi_8 (r + \Phi_4)), \\
 \Phi_{16} &= (\Phi_8 \Phi_{12} + \Phi_7 \Phi_{13}) \omega \alpha_a \Lambda_a \beta_{ah} + \Phi_5 \Phi_7 \mu_a \Lambda_h (\Phi_7 \mu_a - 2 \Phi_8), \\
 \Phi_{17} &= \Phi_3 (\Phi_4 \Phi_{12} \beta_h + \Phi_7 (r + \Phi_4)) + \kappa q \Phi_4 \Phi_7, \quad \Phi_{18} = \Phi_3 \Phi_4 (\theta \Phi_7 - \Phi_1 \Phi_{12}) + \theta \Phi_6 \Phi_7 (\gamma_s + \Phi_4), \\
 \Phi_{19} &= \Phi_1 \Phi_3 \Phi_4 (\Phi_{13} (\theta \Phi_7 - 2 \Phi_{12} \mu_h) + \theta \Phi_8 \Phi_{12}), \quad \Phi_{20} = \Phi_5 \mu_a \Lambda_h (\Phi_7 \Phi_{17} \mu_a - 2 \kappa q \Phi_4 \Phi_7 \Phi_8 - \Phi_3 \Phi_{15}), \\
 \Phi_{21} &= \Phi_3 \Phi_4 (\Phi_7 (\Phi_1 \Phi_{13} - 2 \theta \Phi_8) + \Phi_1 \Phi_8 \Phi_{12}), \quad \Phi_{22} = \theta \Phi_6 (\Phi_8 \Phi_{12} + \Phi_7 \Phi_{13}) \omega \gamma_s - \Phi_{19}, \\
 \Phi_{23} &= (\Phi_7 \Phi_{14} - \Phi_8 \Phi_{13}) \omega \alpha_a \Lambda_a \beta_{ah} + \Phi_5 \Phi_8 \mu_a \Lambda_h (\Phi_8 - 2 \Phi_7 \mu_a), \\
 \Phi_{24} &= -\Phi_3 (\Phi_4 \Phi_7 \Phi_{13} \beta_h + \Phi_8 (\Phi_4 \Phi_{12} \beta_h + 2 \Phi_7 (r + \Phi_4))) - 2 \kappa q \Phi_4 \Phi_7 \Phi_8, \\
 \Phi_{25} &= \Phi_3 \Phi_4 (\Phi_7 (\Phi_1 \Phi_{13} - 2 \theta \Phi_8) + \Phi_1 \Phi_8 \Phi_{12}) - 2 \theta \Phi_6 \Phi_7 \Phi_8 (\gamma_s + \Phi_4), \\
 \Phi_{26} &= \Phi_{25} \mu_a + \Phi_3 \Phi_4 (\theta \Phi_8^2 - \Phi_1 \Phi_{13} \Phi_8 + \Phi_1 \Phi_7 \Phi_{14}) + \theta \Phi_6 \Phi_8^2 (\gamma_s + \Phi_4), \\
 \Phi_{27} &= \Phi_{24} \mu_a + \Phi_3 (\Phi_8 (\Phi_4 \Phi_{13} \beta_h + \Phi_8 (r + \Phi_4)) - \Phi_4 \Phi_7 \Phi_{14} \beta_h) + \kappa q \Phi_4 \Phi_8^2, \\
 \Phi_{28} &= \Phi_{14} (2 \Phi_{12} \mu_h - \theta \Phi_7) + \Phi_{13}^2 (-\mu_h) + \theta \Phi_8 \Phi_{13}, \\
 \Phi_{29} &= \Phi_9 \alpha_h + \Phi_2 (\Phi_6 (\gamma_s + \Phi_4) + \Phi_3 \Phi_4), \quad \Phi_{30} = \Phi_1 \Phi_3 \Phi_4 (2 \Phi_{13} \mu_h - \theta \Phi_8) + \theta \Phi_6 \Phi_8 \omega \gamma_s, \\
 \Phi_{31} &= \Phi_3 \Phi_4 \Phi_5 \mu_a \beta_h \Lambda_h (\Phi_7 \mu_a - \Phi_8), \quad \Phi_{32} = \Phi_{30} \alpha_a \Lambda_a \beta_{ah} + \Phi_1 \Phi_3 \Phi_4 \Phi_5 \mu_a \Lambda_h (\Phi_8 - \Phi_7 \mu_a).
 \end{aligned}
 \tag{11}$$

The coefficient  $k_1$  is positive and  $k_5$  can be positive when  $\mathcal{R}_1 < 1$ , and  $\mathcal{R}_2 < 1$ . The signs of the coefficients  $k_2$ ,  $k_3$  and  $k_4$  determine the existence of possible positive real roots. To get this, we can apply the Descartes Rule of Signs to  $g(z) = k_1 z^4 + k_2 z^3 + k_3 z^2 + k_4 z + k_5$  as given in (9) (with  $z = \lambda_a^*$ ). The expected number of positive real roots from  $g(z)$  is shown in Table 2 while Theorem 3 summarizes the findings of Table 2.

*Theorem 3 The mpox model (3) exhibits*

- (1) No EE if  $\mathcal{R}_0 < 1$ , and sign changes (case 1)
- (2) Exists backward bifurcation if  $\mathcal{R}_0 < 1$ , and two sign changes (cases 3, 5, 7), giving 0, or 2 endemic equilibria
- (3) Unique EE if  $\mathcal{R}_0 > 1$ , and one sign change (Cases 2, 4, 6)
- (4) Multiple EE (1, or 3) if  $\mathcal{R}_0 > 1$ , and three sign changes (Case 8)

Table 2, which is summarized in Theorem 3, shows that backward bifurcation exists under cases 3, 5, and 7 when  $\mathcal{R}_0 < 1$ , while a multiple endemic equilibria exist when  $\mathcal{R}_0 > 1$  and the case 4 holds. When  $\mathcal{R}_0 > 1$ , and cases 2, 4, and 6 hold, then we have a unique endemic equilibrium, otherwise case 1 shows the existence of no endemic equilibria. The existence of the backward bifurcation is shown in Fig. 2 under the case (2) of Theorem 3. Backward bifurcation in the mpox model (3) has significant epidemiological implications, indicating that the usual condition of  $\mathcal{R}_0 < 1$  is no longer sufficient for mpox elimination, though it remains essential. In such scenarios, mpox elimination may depend on the initial subpopulation sizes. Thus, controlling mpox when  $\mathcal{R}_0 < 1$  may require considering the starting sizes of specific subpopulations.

### Evaluating mpox model global stability of endemic equilibrium

Here, we evaluate the global asymptotic stability of the mpox model (3) for a special case when  $\omega = 0$ , allowing us to omit the  $R_h$  compartment without any loss of generality, as it is independent of the remaining model Eq. (3). We will first present the endemic equilibrium at a steady state,  $D_1$ , for the mpox model (3) as follows:

Case	$k_1$	$k_2$	$k_3$	$k_4$	$k_5$	$\mathcal{R}_0$	Sign changes	No. of EPRR (EE)
1	+	+	+	+	+	$\mathcal{R}_0 < 1$	0	0
2	+	+	+	-	-	$\mathcal{R}_0 > 1$	1	1
3	+	-	-	+	+	$\mathcal{R}_0 < 1$	2	0, 2
4	+	-	-	-	-	$\mathcal{R}_0 > 1$	1	1
5	+	+	-	+	+	$\mathcal{R}_0 < 1$	2	0, 2
6	+	+	-	-	-	$\mathcal{R}_0 > 1$	1	1
7	+	-	+	+	+	$\mathcal{R}_0 < 1$	2	0, 2
8	+	-	+	-	-	$\mathcal{R}_0 > 1$	3	1, 3

**Table 2.** The expected positive real roots (EPRR) associated with  $g(z)$  for various cases of  $\mathcal{R}_1$ , and  $\mathcal{R}_2$

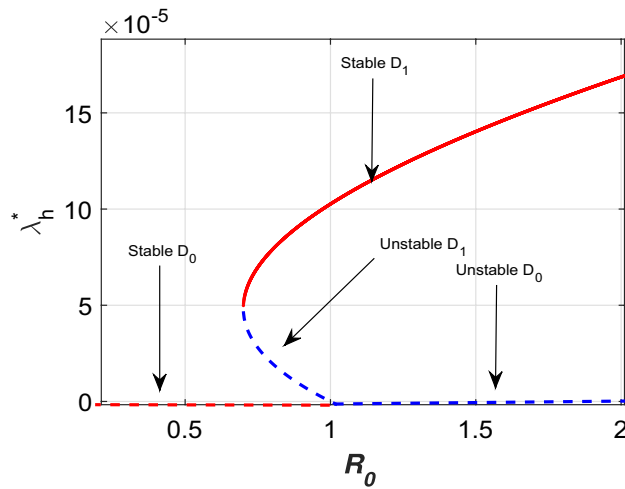


**Fig. 2.** The plot describes the backward bifurcation diagram for model (3). The bold red line indicates the stable endemic equilibrium  $D_1$ , the red dashed line on the x-axis shows the stable disease-free equilibrium  $D_0$ , the blue dashed line on the x-axis represents the unstable  $D_0$ , while the blue dashed line on the vertical y-axis indicates the unstable  $D_1$

$$\begin{aligned}
 \Lambda_h &= \theta \lambda_h^* S_h^* + \mu_h S_h^*, \\
 \theta \lambda_h^* S_h^* &= (\alpha_h + x\rho + \tau + \mu_h) E_h^*, \\
 \alpha_h E_h^* &= (r + \delta_h + \kappa q + \mu_h) I_h^*, \\
 (\gamma_s + \mu_h) S_{fih}^* &= (x\rho + \tau) E_h^* + \kappa q I_h^*, \\
 \Lambda_a &= \lambda_a S_a^* + \mu_a S_a^*, \\
 \lambda_a^* S_a^* &= (\alpha_a + \mu_h) E_a^*, \\
 \mu_a I_a^* &= \alpha_a E_a^*.
 \end{aligned}
 \tag{12}$$

The formulation presented in (12) will be utilized to prove the global asymptotic stability of the endemic equilibrium (EE),  $D_1$ .

*Theorem 4* Mpox model (3) is globally asymptotically stable (GAS) whenever  $\mathcal{R}_0 > 1$

*Proof* First of all, we consider the Lyapunov function given by

$$\begin{aligned}
 \mathcal{L}(t) &= S_h - S_h^* - S_h^* \ln \left( \frac{S_h}{S_h^*} \right) + E_h - E_h^* - E_h^* \ln \left( \frac{E_h}{E_h^*} \right) + \frac{\beta_h I_h^* S_h^*}{\alpha_h E_h^*} \left[ I_h - I_h^* - I_h^* \ln \left( \frac{I_h}{I_h^*} \right) \right] + \frac{\beta_{ah} I_a^* S_h^*}{(x\rho + \tau) + \kappa q} \\
 &\times \left[ S_{fih} - S_{fih}^* - S_{fih}^* \ln \left( \frac{S_{fih}}{S_{fih}^*} \right) \right] + S_a - S_a^* - S_a^* \ln \left( \frac{S_a}{S_a^*} \right) + E_a - E_a^* - E_a^* \ln \left( \frac{E_a}{E_a^*} \right) \\
 &+ \frac{\beta_a I_a^* S_a^*}{\alpha_a E_a^*} \left[ I_a - I_a^* - I_a^* \ln \left( \frac{I_a}{I_a^*} \right) \right]
 \end{aligned}
 \tag{13}$$

Time derivative of Eq. (13) is obtained as

$$\begin{aligned}
 \dot{\mathcal{L}} &= \left( 1 - \frac{S_h^*}{S_h} \right) \dot{S}_h + \left( 1 - \frac{E_h^*}{E_h} \right) \dot{E}_h + \frac{\beta_h I_h^* S_h^*}{\alpha_h E_h^*} \left( 1 - \frac{I_h^*}{I_h} \right) \dot{I}_h + \frac{\beta_{ah} I_a^* S_h^*}{(x\rho + \tau) + \kappa q} \left( 1 - \frac{S_{fih}^*}{S_{fih}} \right) \dot{S}_{fih} \left( 1 - \frac{S_a^*}{S_a} \right) \dot{S}_a \\
 &+ \left( 1 - \frac{E_a^*}{E_a} \right) \dot{E}_a + \frac{\beta_a I_a^* S_a^*}{\alpha_a E_a^*} \left( 1 - \frac{I_a^*}{I_a} \right) \dot{I}_a
 \end{aligned}
 \tag{14}$$

The formulation on the right-hand side of Eq. (14) is evaluated by utilizing the equations from the mpox model (3) as follows:

$$\begin{aligned}
 \left(1 - \frac{S_h^*}{S_h}\right) \dot{S}_h &= \left(1 - \frac{S_h^*}{S_h}\right) \left[ \Lambda_h - \left(\frac{\beta_{ah}I_a}{N_h} + \frac{\beta_h I_h}{N_h}\right) S_h - \mu_h S_h \right], \\
 &\leq \left(1 - \frac{S_h^*}{S_h}\right) [\Lambda_h - (\beta_{ah}I_a + \beta_h I_h)S_h - \mu_h S_h], \\
 &\leq \left(1 - \frac{S_h^*}{S_h}\right) [(\beta_{ah}I_a^* + \beta_h I_h^*)S_h^* + \mu_h S_h^* - (\beta_{ah}I_a + \beta_h I_h)S_h - \mu_h S_h], \\
 &\leq \mu_h S_h^* \left(2 - \frac{S_h^*}{S_h} - \frac{S_h}{S_h^*}\right) + \beta_{ah}I_a^* S_h^* \left(1 - \frac{S_h^*}{S_h} - \frac{I_a S_h}{I_a^* S_h^*} + \frac{I_a}{I_a^*}\right) + \beta_h I_h^* S_h^* \left(1 - \frac{S_h^*}{S_h} - \frac{I_h S_h}{I_h^* S_h^*} + \frac{I_h}{I_h^*}\right), \\
 &\leq \beta_{ah}I_a^* S_h^* \left(1 - \frac{S_h^*}{S_h} - \frac{I_a S_h}{I_a^* S_h^*} + \frac{I_a}{I_a^*}\right) + \beta_h I_h^* S_h^* \left(1 - \frac{S_h^*}{S_h} - \frac{I_h S_h}{I_h^* S_h^*} + \frac{I_h}{I_h^*}\right)
 \end{aligned} \tag{15}$$

$$\begin{aligned}
 \left(1 - \frac{E_h^*}{E_h}\right) \dot{E}_h &= \left(1 - \frac{E_h^*}{E_h}\right) [(\beta_{ah}I_a + \beta_h I_h)S_h - \Phi_1 E_h], \\
 &= \left(1 - \frac{E_h^*}{E_h}\right) [(\beta_{ah}I_a + \beta_h I_h)S_h - (\beta_{ah}I_a^* + \beta_h I_h^*)S_h^* \frac{E_h}{E_h^*}], \\
 &= \beta_{ah}I_a^* S_h^* \left(1 - \frac{E_h}{E_h^*} + \frac{I_a S_h}{I_a^* S_h^*} - \frac{I_a S_h E_h^*}{I_a^* S_h^* E_h}\right) + \beta_h I_h^* S_h^* \left(1 - \frac{E_h}{E_h^*} + \frac{I_h S_h}{I_h^* S_h^*} - \frac{I_h S_h E_h^*}{I_h^* S_h^* E_h}\right), \\
 \frac{\beta_a I_h^* S_h^*}{\alpha_h E_h^*} \left(1 - \frac{I_h^*}{I_h}\right) \dot{I}_h &= \frac{\beta_h I_h^* S_h^*}{\alpha_h E_h^*} \left(1 - \frac{I_h^*}{I_h}\right) [\alpha_h E_h - \Phi_2 I_h], \\
 &= \frac{\beta_a I_h^* S_h^*}{E_h^*} \left(1 - \frac{I_h^*}{I_h}\right) \left[E_h - \frac{E_h^*}{I_h^*} I_h\right], \\
 &= \beta_h I_h^* E_h^* \left(1 - \frac{I_h}{I_h^*} - \frac{E_h I_h^*}{E_h^* I_h} + \frac{E_h}{E_h^*}\right),
 \end{aligned} \tag{16}$$

$$\begin{aligned}
 \frac{\beta_{ah}I_h^* S_h^*}{(x\rho + \tau) + \kappa q} \left(1 - \frac{S_{fih}^*}{S_{fih}}\right) \dot{S}_{fih} &= \frac{\beta_{ah}I_h^* S_h^*}{(x\rho + \tau) + \kappa q} \left(1 - \frac{S_{fih}^*}{S_{fih}}\right) [(x\rho + \tau)E_h + \kappa q I_h - \Phi_3 S_{fih}], \\
 &= \frac{\beta_{ah}I_h^* S_h^*}{E_h^* + I_h^*} \left[E_h + I_h - \frac{E_h^*}{S_{fih}^*} S_{fih}\right], \\
 &= \beta_{ah}I_a^* S_h^* \left(1 + \frac{E_h}{E_h^*} + \frac{I_h}{I_h^*} - \frac{E_h S_{fih}^*}{E_h^* S_{fih}} - \frac{S_{fih}}{S_{fih}^*}\right),
 \end{aligned} \tag{17}$$

$$\begin{aligned}
 \left(1 - \frac{S_a^*}{S_a}\right) \dot{S}_a &\leq \left(1 - \frac{S_a^*}{S_a}\right) [\Lambda_a - (\beta_2 I_h + \beta_a I_a)S_a - \mu_a S_a] \\
 &= \left(1 - \frac{S_a^*}{S_a}\right) [(\beta_2 I_h^* + \beta_a I_a^*)S_a^* + \mu_a S_a^* - (\beta_2 I_h + \beta_a I_a)S_a - \mu_a S_a] \\
 &= \mu_a S_a^* \left(2 - \frac{S_a^*}{S_a} - \frac{S_a}{S_a^*}\right) + \beta_2 I_h^* S_a^* \left(1 - \frac{S_a^*}{S_a} - \frac{I_a S_a}{I_a^* S_a^*} + \frac{I_a}{I_a^*}\right) + \beta_a I_a^* S_a^* \left(1 - \frac{S_a^*}{S_a} - \frac{I_a S_a}{I_a^* S_a^*} + \frac{I_a}{I_a^*}\right),
 \end{aligned} \tag{18}$$

$$\begin{aligned}
 \left(1 - \frac{E_a^*}{E_a}\right) \dot{E}_a &\leq \left(1 - \frac{E_a^*}{E_a}\right) [\beta_2 I_h + \beta_a I_a - \Phi_5 E_a] \\
 &\leq \left(1 - \frac{E_a^*}{E_a}\right) \left[\beta_2 I_h + \beta_a I_a - \frac{\beta_2 I_h^* S_a^* E_a^*}{E_a^*} - \frac{\beta_a I_a^* S_a^* E_a^*}{E_a^*}\right] \\
 &\leq \beta_2 I_h^* S_a^* \left(1 - \frac{E_a}{E_a^*} + \frac{I_a S_a}{I_a^* S_a^*} - \frac{I_a S_a E_a^*}{E_a I_a^* S_a^*}\right) + \beta_a I_a^* S_a^* \left(1 - \frac{E_a}{E_a^*} + \frac{I_a S_a}{I_a^* S_a^*} - \frac{I_a S_a E_a^*}{E_a I_a^* S_a^*}\right),
 \end{aligned} \tag{19}$$

$$\begin{aligned}
 \frac{\beta_a I_a^* S_a^*}{\alpha_a E_a^*} \left(1 - \frac{I_a^*}{I_a}\right) \dot{I}_a &\leq \frac{\beta_a I_a^* S_a^*}{\alpha_a E_a^*} \left(1 - \frac{I_a^*}{I_a}\right) [\alpha_a E_a - \mu_a I_a] \\
 &\leq \frac{\beta_a I_a^* S_a^*}{\alpha_a E_a^*} \left(1 - \frac{I_a^*}{I_a}\right) \left[E_a - \frac{E_a^*}{I_a^*} I_a\right] \\
 &\leq \beta_a I_a^* S_a^* \left(1 - \frac{E_a}{E_a^*} + \frac{I_a E_a}{I_a^* E_a^*} - \frac{I_a}{I_a^*}\right).
 \end{aligned} \tag{20}$$

Putting Eqs. (15)–(21) into (14), and after further algebraic simplification, we obtain

$$\begin{aligned} \mathcal{L} = & \beta_{ah} I_a^* S_h^* \left( 3 - \frac{S_h^*}{S_h} - \frac{S_{fih}}{S_{fih}^*} + \frac{I_a}{I_a^*} - \frac{E_h S_{fih}^*}{E_h^* S_{fih}} - \frac{I_a S_h E_h^*}{E_h I_a^* S_h^*} \right) + \beta_h I_h^* S_h^* \left( 3 - \frac{S_h^*}{S_h} - \frac{E_h I_h^*}{I_h E_h^*} - \frac{I_h S_h E_h^*}{E_h I_h^* S_h^*} \right) \\ & + \beta_2 I_h^* S_a^* \left( 3 - \frac{S_a^*}{S_a} - \frac{E_a I_a^*}{I_a E_a^*} - \frac{I_a S_a E_a^*}{E_a I_a^* S_a^*} \right) + \beta_a I_a^* S_a^* \left( 3 - \frac{S_a^*}{S_a} - \frac{E_a I_a^*}{I_a E_a^*} - \frac{I_a S_a E_a^*}{E_a I_a^* S_a^*} \right). \end{aligned} \quad (22)$$

Utilizing the properties of arithmetic and geometric means, we get

$$\begin{aligned} \left( 3 - \frac{S_h^*}{S_h} - \frac{E_h I_h^*}{I_h E_h^*} - \frac{I_h S_h E_h^*}{E_h I_h^* S_h^*} \right) & \leq 0, \\ \left( 3 - \frac{S_a^*}{S_a} - \frac{E_a I_a^*}{I_a E_a^*} - \frac{I_a S_a E_a^*}{E_a I_a^* S_a^*} \right) & \leq 0, \\ \left( 3 - \frac{S_h^*}{S_h} - \frac{S_{fih}}{S_{fih}^*} + \frac{I_a}{I_a^*} - \frac{E_h S_{fih}^*}{E_h^* S_{fih}} - \frac{I_a S_h E_h^*}{E_h I_a^* S_h^*} \right) & \leq 0. \end{aligned}$$

Hence, the largest invariant subset for which  $\mathcal{L} \leq 0$  is  $D_1$ . Therefore, from the results presented in<sup>27</sup>,  $D_1$  is GAS whenever  $\mathcal{R}_0$  is above one.  $\square$

### Estimation of parameters

There were many mpox outbreaks recorded around the globe, in Africa, and the rest of the world. At the beginning of 2022, more than 40 countries faced an outbreak of mpox. Results from June 2024 show that 97,281 confirmed cases were reported for 2022–2023 across 118 countries<sup>28</sup>. Here, we highlight some of the recent outbreaks, namely in the UK (2022) and the United States (2022). Mpox cases in the UK were reported to be 3732, beginning with a traveler from Nigeria who introduced the virus<sup>29</sup>. The cases peaked in July 2022, reaching a total of 1339 that month. The basic reproduction number was around 2.32 for the UK cases. In this outbreak, no death cases were reported. The 2022–2023 mpox outbreak in the United States was part of the global pandemic caused by the West African mpox virus. After identification of the first reported case in Boston, Massachusetts, on May 17, 2022<sup>30</sup>, the infection spread to more cities by August 2022. A high number of mpox cases were reported by the USA worldwide, compared to other countries, with California reporting the most cases<sup>31</sup>. A death due to mpox was reported on August 30, 2022<sup>32</sup>.

This section details the parameter estimations for the mpox disease model (3), based on actual cases reported from the US from January 1, 2024, to August 31, 2024. The data has been sourced from the Centers for Disease Control and Prevention, as referenced in<sup>33,34</sup>, and represents daily reported cases. In this data fitting, we consider the well-known method of data fitting known as the nonlinear least squares technique for curve fitting to the differential equation system. To estimate the initial conditions of the human population, we consider the total human population of the US based on 2024 to be  $N_h(0) = 345,426,571$ . The healthy (susceptible) population in the absence of disease is estimated as,  $S_h(0) = 345,426,064$ . The number of individuals that are exposed,  $E_h(0) = 500$  (this is assumed to be for the best fit, as there is no such details for the exposed cases), the mpox cases reported in the US, is  $I_h(0) = 7$ . The self-isolated and recovered individuals are  $S_{fih}(0) = R_h(0) = 0$ . The initial conditions for the animals population are assumed based on model fitting, as no such data is available. The total animal population is taken as  $N_a(0) = 14350$ , where  $S_a(0) = 14000$ ,  $E_a(0) = 300$ , and  $I_a(0) = 50$ .

Among the model parameters, some can be computed directly from the model's existing equations, whereas others are fitted to the model. One parameter obtained from the literature, is the average lifespan of people in the United states of America, which is  $1/(79.25 \times 365)$  per day<sup>35</sup>. The model equation can be used to derive the natural birth rate, given by the formula  $\Lambda_h = \mu_h \times N_h(0)$ , which is approximately  $\Lambda_h \approx 11942$ . Likewise, it is assumed that the average lifespan of animal (e.g., rodents) is  $\mu_a = 1/(5 \times 365)$  per day, where the total lifespan of the animals (e.g., rodents) is 5 years; it may change due to species. Using the relation  $\Lambda_a = \mu_a \times N_a(0)$ , we can compute the birth rate for the rodent population. The remaining parameters are derived from the data fitting experiment for the mpox disease model (3), which are listed in Table 3 with a daily time unit. The basic reproduction number,  $\mathcal{R}_0 \approx 1.0937$ , is calculated using the parameter values presented obtained using the parameter values presented in Table 3. The Root Mean Square Error (RMSE) is 11.4284. The numerical value of the basic reproduction number aligns well with the mpox outbreak situation in the USA, as noted in<sup>33</sup>. The basic reproduction number throughout the mpox outbreak was found to be less than 1. The graphical result shown in Fig. 3 illustrates the observed cases versus model fitting. Figure 4 represents the daily cases comparison in the experiment and their corresponding residuals.

### Sensitivity analysis

The development of mathematical models in disease epidemiology primarily aims to facilitate the control and prevention of infectious diseases. To get this, it is crucial to identify and manage the parameters that significantly influence both the model equations and the basic reproduction number  $\mathcal{R}_0$ . The model dynamics involve calculating the sensitivity indices (SI) through the normalized forward sensitivity indices (NFSI)<sup>36</sup>. For a given parameter  $\phi$ , the sensitivity index is calculated using the formula:  $\prod_{\phi}^{\mathcal{R}_0} = \frac{\partial \mathcal{R}_0}{\partial \phi} \times \frac{\phi}{\mathcal{R}_0}$ . The sensitivity indices derived for  $\mathcal{R}_0$  are presented in Table 4, with their graphical representation shown in Fig. 5. Based on the results in Table 4, the parameters  $\beta_a, \mu_a, \alpha_a, \theta, \kappa, \Lambda_a$ , and others are identified as the most influential factors affecting both the model dynamics and  $\mathcal{R}_0$ .

Biological interpretations	Parameter	Value	Unit	range	source
Animal human contact	$\beta_{ah}$	0.6929	per contact	0.3–0.9	Data fitting
human to humans contact	$\beta_h$	0.2216	per contact	0.1–0.4	Data fitting
Humans to animal contact	$\beta_2$	0.0106	per contact	0.005–0.02	Data fitting
Animal to animal contact	$\beta_a$	0.0023	per contact	0.001–0.01	Data fitting
Vigilance efficacy	$\theta$	0.1686	day <sup>-1</sup>	0.1–0.3	Data fitting
Waning immunity	$\omega$	0.0101	day <sup>-1</sup>	0.005–0.03	Data fitting
Progress from exposed to infections	$x$	0.0085	day <sup>-1</sup>	0.005–0.02	Data fitting
Tested rate of exposed people	$\rho$	0.4600	day <sup>-1</sup>	0.3–0.6	Data fitting
Humans incubation duration	$\alpha_h$	0.0237	day <sup>-1</sup>	0.02–0.05	Data fitting
Tracing and testing exposed humans	$\tau$	0.0100	day <sup>-1</sup>	0.005–0.03	Data fitting
People adopt self-isolation	$\kappa$	0.0115	day <sup>-1</sup>	0.005–0.02	Data fitting
Isolation rate of infected people	$q$	0.5550	day <sup>-1</sup>	0.2–0.7	Data fitting
Recovery rate of non-isolated infected humans	$r$	0.0124	day <sup>-1</sup>	0.005–0.03	Data fitting
Humans disease death rate	$\delta_h$	0.0124	day <sup>-1</sup>	0.005–0.02	Data fitting
Rate of recovery of isolated infected humans	$\gamma_s$	0.0100	day <sup>-1</sup>	0.005–0.02	Data fitting
Mammal incubation period	$\alpha_a$	0.0520	day <sup>-1</sup>	0.03–0.07	Data fitting

**Table 3.** Details of the parameters and their numerical value.

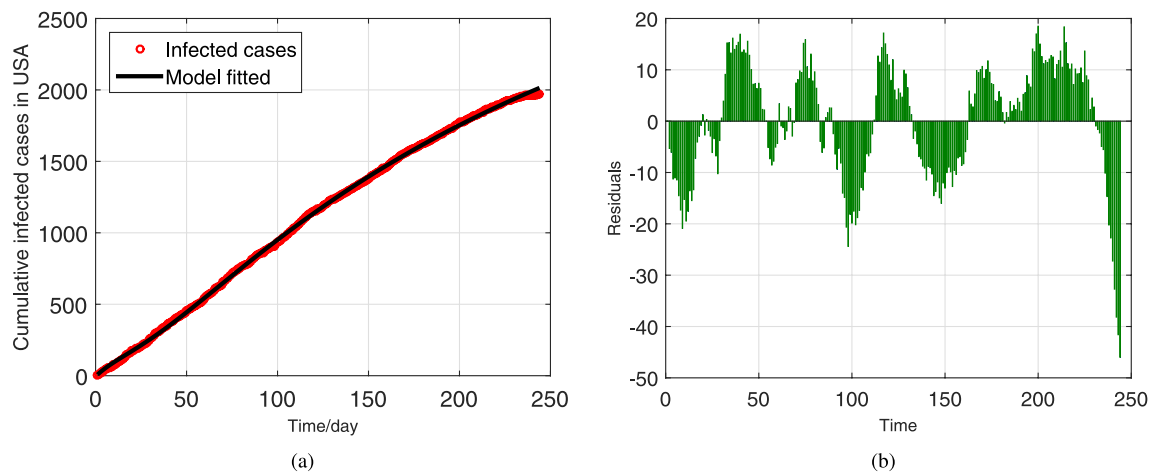


**Fig. 3.** The plot shows the data fitting to the model. In subfigure (a), the model is compared to the data, with the bold line representing the model's solution and the circles denoting the actual reported cases from the USA. Subfigure (b) presents the corresponding residuals.

From this analysis, it is clear that  $\beta_a$  and  $\mu_a$  are the most sensitive parameters. Effective control strategies should focus on reducing  $\beta_a$  (e.g., through preventive measures like reducing transmission), or managing  $\mu_a$  (through improved healthcare to lower the death rate) to achieve a substantial impact on the disease's spread.

### Numerical results

The numerical simulations, carried out using the Runge-Kutta fourth-order method, provide insights into the dynamics of mpox transmission between humans and mammals under varying parameter conditions. The model incorporates critical aspects such as self-isolation, testing, and public awareness, which significantly impact the spread of the virus. Key results are discussed below in the context of the parameters defined in the model:

#### Impact of transmission probabilities ( $\beta_{ah}$ and $\beta_h$ )

Figures 6 and 7 illustrate the effects of varying  $\beta_{ah}$  (probability of transmission from infected mammals to humans) and  $\beta_h$  (probability of transmission between humans). These parameters directly influence the force of infection ( $\lambda_h$ ) in humans. As  $\beta_{ah}$  and  $\beta_h$  increase, the number of exposed, infected, and self-isolated individuals rises, indicating a higher rate of new infections. This highlights the role of close contact with infected individuals

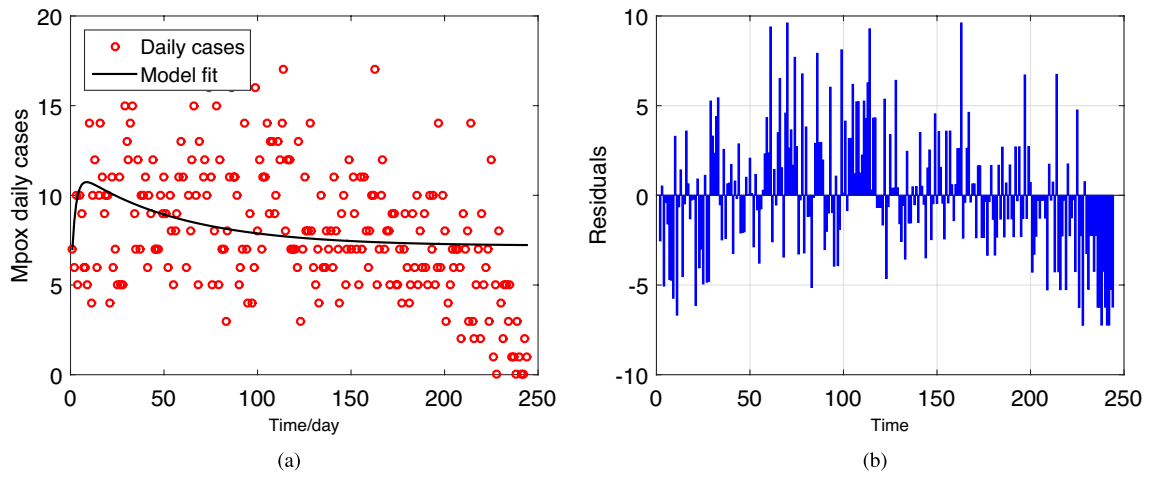


**Fig. 4.** The plot shows the data fitting to the model. In subfigure (a), the model is compared to the daily cases, with the bold line representing the model’s solution and the circles denoting the actual reported cases from the USA. Subfigure (b) presents the corresponding residuals.

Symbol	SI	Symbol	SI
$\beta_{ah}$	0.001314	$\Lambda_a$	0.001314
$\beta_h$	0.002904	$\Lambda_h$	-0.001314
$\beta_2$	0.001314	$\mu_a$	-1.03398
$\beta_a$	1	$\mu_h$	0.001306
$\theta$	0.004219	$x$	-0.000438
$\rho$	-0.000438	$\alpha_h$	0.001562
$\tau$	-0.001120	$\kappa$	-0.001574
$q$	-0.000942	$r$	-0.000942
$\delta_h$	-0.001697	$\alpha_a$	0.036880

**Table 4.** Normalized sensitivity indices of  $\mathcal{R}_0$ .

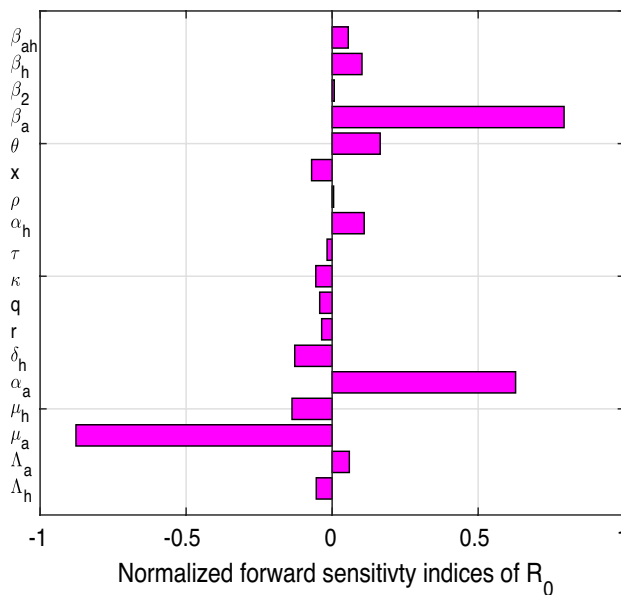


**Fig. 5.** The normalized forward sensitivity analysis of  $\mathcal{R}_0$ .

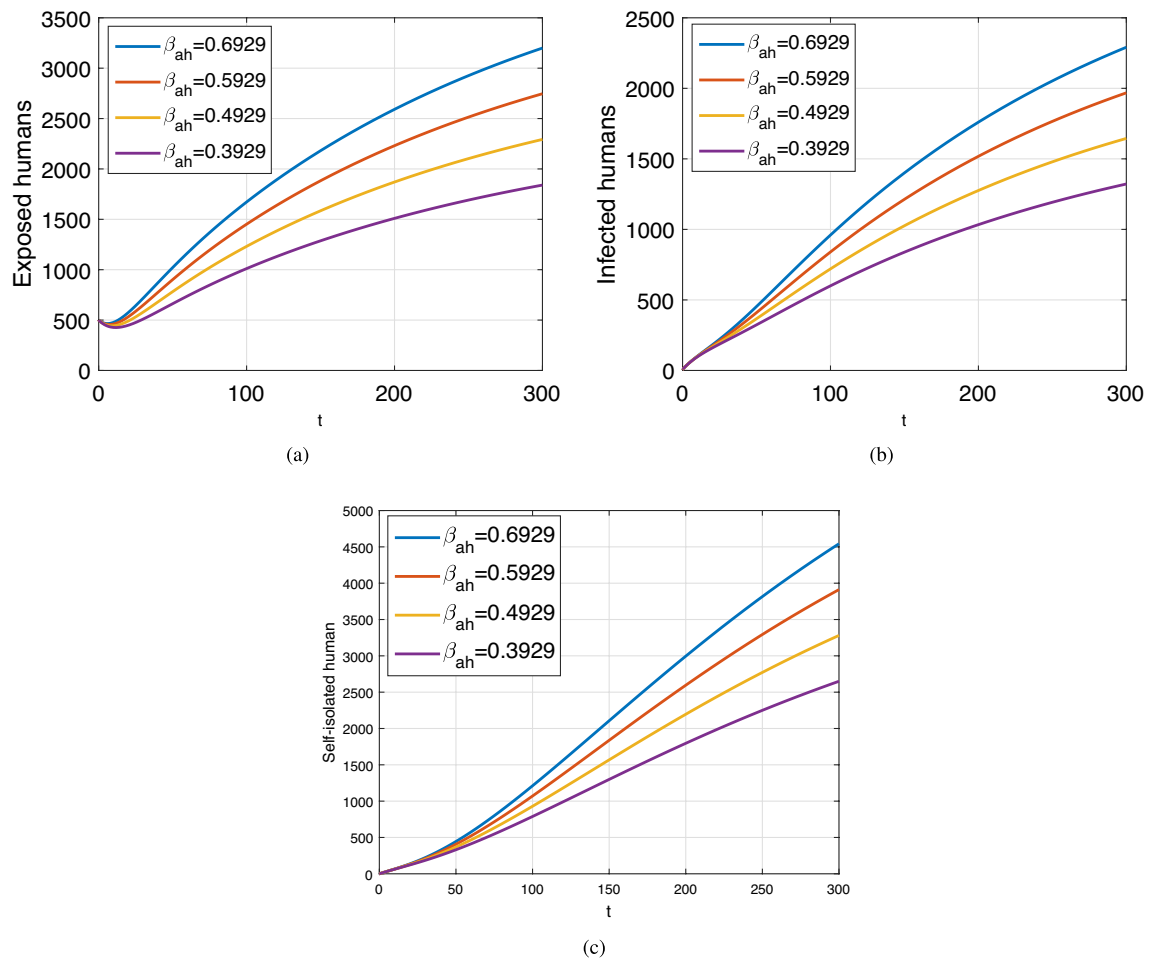


**Fig. 6.** The plot describes the dynamics of the exposed, infected and self-isolated humans individuals under varying values of  $\beta_{ah}$ . Subfigures (a–c) show the trajectories of the exposed, infected and self-isolated people, respectively.

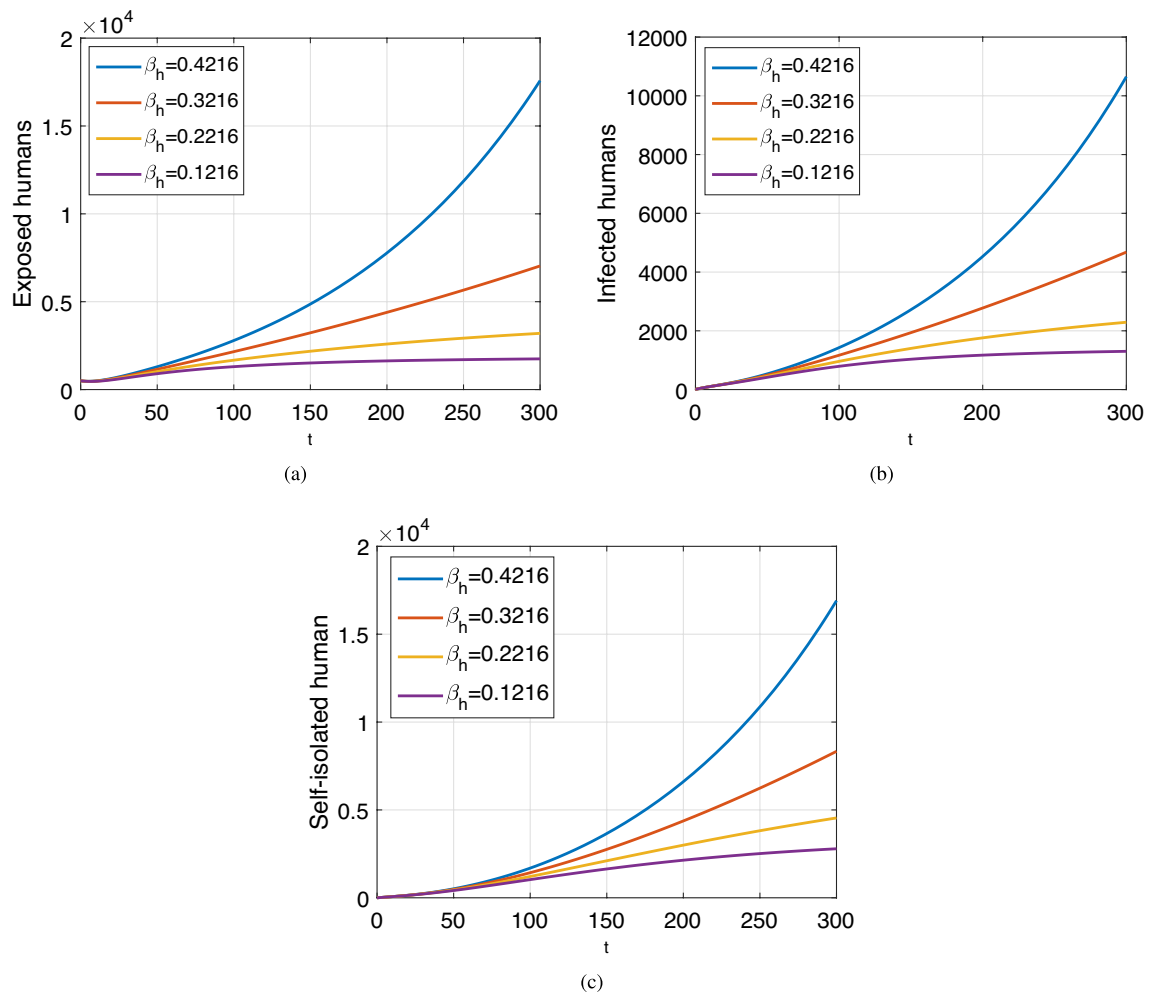
or mammals in driving the outbreak. The effectiveness of mitigation strategies, such as reducing contact rates through testing and isolation, is particularly crucial when these transmission probabilities are high.

Figure 8 illustrates the dynamics of exposed, infected, and self-isolated human populations under varying values of the transmission parameter  $\beta_a$ , which represents the probability that contact with infected mammals results in a new human infection. Sub-figures (a), (b), and (c) respectively depict the time evolution of the exposed, infected, and self-isolated human population. Figure 8a shows that higher values of  $\beta_a$  results in a steeper rise in exposed population, indicating accelerated transmission from mammals. In Fig. 8b, the infected population increases more rapidly and peaks earlier with higher  $\beta_a$ , suggesting quicker spread and prolonged persistence of the disease. Figure 8c reveals that as  $\beta_a$  increases, the self-isolated population also peaks sooner, reflecting a stronger response in isolating affected individuals. Over all, Fig. 8 emphasizes the impact of  $\beta_a$  on the spread of mpox, highlighting the importance of timely testing, awareness, and isolation to control the outbreak.

### Role of awareness and vigilance

Figure 9 demonstrates how the parameter  $\theta$ , which represents the efficacy of public awareness in reducing susceptibility, affects mpox disease dynamics. Higher values of  $\theta$  indicate a more vigilant population that actively avoids exposure to the virus. Increased vigilance reduces the number of susceptible individuals transitioning to the exposed class. This demonstrates the importance of awareness campaigns and educational initiatives in reducing the spread of mpox. The results underscore that even partial awareness ( $\theta \neq 1$ ) can substantially curb the outbreak, making it a valuable intervention strategy.

Figure 10 shows the dynamics of the exposed and infected population for different values of  $q$ , which represents the isolation rate of infectious individuals. In Fig. 10a, as  $q$  increases, the peak of the exposed individuals decreases, suggesting that high isolation rates effectively reduce the number of people progressing from exposure to infection. Figure 10b indicates a similar trend for the infected individuals, where an increase in  $q$  leads to a lower peak and a quicker decline in the infected population, highlighting the role of effective isolation in controlling the spread of the mpox virus among humans. Overall, the results in Fig. 10 underscore the significance of increasing the isolation measure to reduce the transmission and spread of the infection.



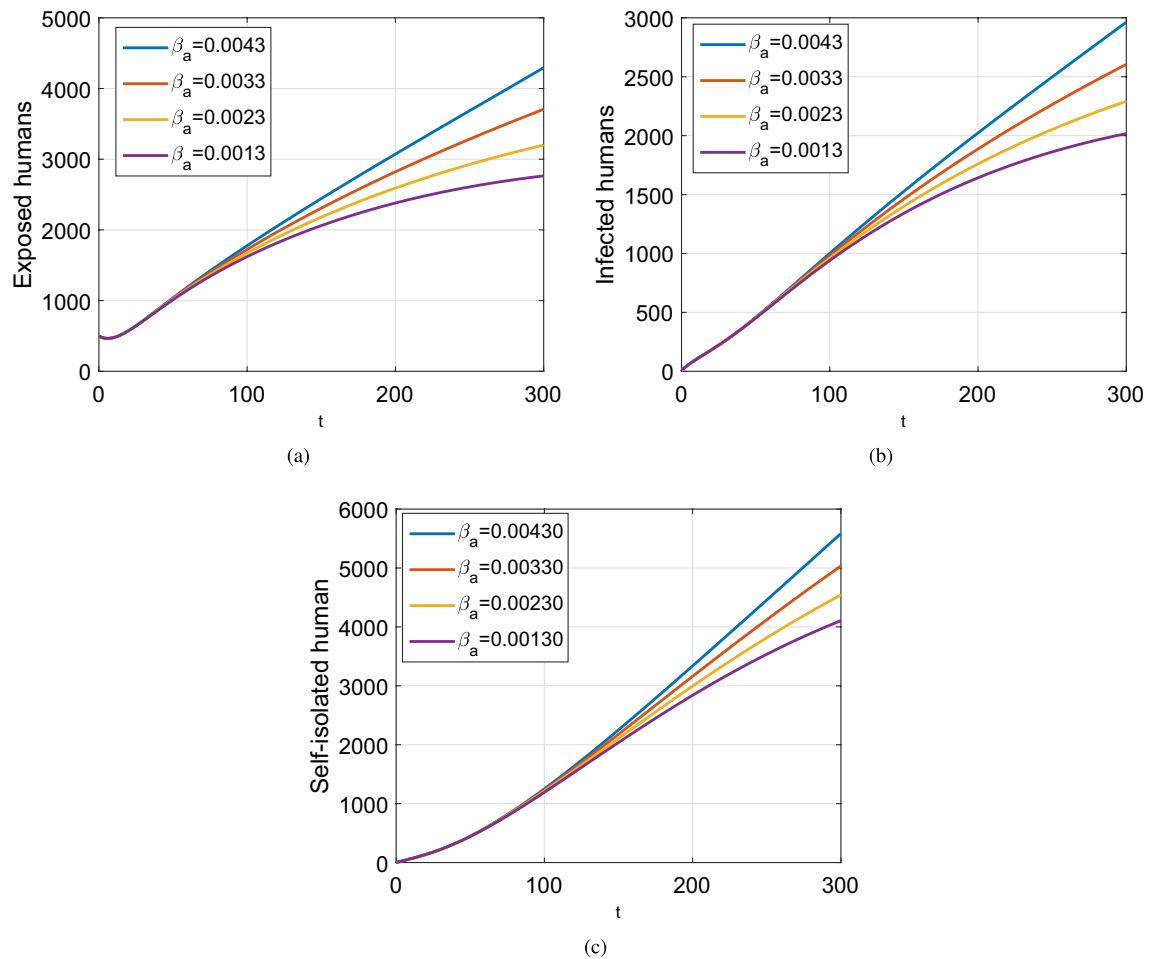
**Fig. 7.** The plot describes the dynamics of the exposed, infected, and self-isolated human individuals under varying values of  $\beta_h$ . Specifically, subfigures (a), (b), and (c) depict the temporal changes in the numbers of exposed, infected, and self-isolated people, respectively. Variations in  $\beta_h$  represent changes in the human-to-human transmission rate, demonstrating how this parameter influences disease progression across the compartments.

Figure 11 illustrates the dynamics of exposed and infected human populations for varying values of  $\kappa$ , representing the fraction of infectious individuals. In Fig. 11a, increasing  $\kappa$  reduces the peak of the exposed population, indicating that higher self-isolation rates among infectious individuals lead to fewer exposures progressing to infection. Figure 11b shows a similar trend for the infected population, where higher values of  $\kappa$  result in a lower peak and a faster decline in infections. These results demonstrate the importance of encouraging self-isolation among infected individuals to effectively control the spread of the mpox virus.

Figure 12 represents the impact of the parameter  $\rho$  on the population of exposed and infected humans. It shows that increasing the testing of people will identify the number of individuals, and hence, a reduction will occur. Therefore, improving testing and identifying people who are positive for the virus should lead to their isolation, and those infected should be treated in order to reduce future cases of mpox infection.

Figure 13 represents the impact of the parameter  $\tau$  on the population of exposed and infected humans. It shows that increasing the time to trace exposed people will decrease the population of exposed and infected individuals in the human population. The result given in subfigures (a) and (b) of Fig. 13 clearly shows that when the value of  $\tau$  increases, the number of infected and exposed humans significantly decreases.

The numerical and sensitivity analyses offer critical insights that directly inform public health strategies to combat mpox outbreaks. By identifying the parameters that have a great impact on disease transmission, these findings enable policymakers to prioritize interventions where they will have the most impactful results. The analysis reveals that transmission rates between animals and between humans, along with isolation effectiveness, are the key drivers of outbreak dynamics. This suggests that public health resources should be strategically allocated to enhance surveillance and testing programs, particularly for high-risk populations such as individuals with multiple sex partners or weakened immune systems.



**Fig. 8.** The plot describes the dynamics of exposed, infected, and self-isolated individuals for different values of  $\beta_a$ . Subfigures (a), (b), and (c) display the temporal changes in the number of exposed, infected, and self-isolated people, respectively.

The model further demonstrates that even modest improvements in testing and isolation rates can significantly reduce infection peaks, thereby highlighting the importance of investing in accessible diagnostic services and effective quarantine infrastructure.

Public awareness campaigns also emerge as critical, as demonstrated by the influence of parameter  $\theta$ . Enhancing awareness and educating communities about disease prevention can substantially reduce the susceptible population and slow transmission. Additionally, the strong influence of zoonotic transmission highlights the need for integrated One-Health approaches that monitor and control potential animal reservoirs in endemic regions. These evidence-based recommendations provide a framework for optimizing outbreak response efforts through targeted, data-driven interventions.

## Conclusion

Based on the results obtained from the mathematical modeling and analysis of mpox dynamics, the study provides crucial insights into the impact of non-pharmaceutical interventions (especially self-isolation, testing, and public awareness) in controlling the spread of the disease. The model effectively captures the dynamics of mpox transmission between humans and mammals, demonstrating that the basic reproduction number  $\mathcal{R}_0$  serves as a key threshold parameter. When  $\mathcal{R}_0 < 1$ , the model indicates that the mpox-free equilibrium is locally asymptotically stable, suggesting that the disease will eventually die out. Conversely, if  $\mathcal{R}_0 > 1$ , the possibility of a stable endemic equilibrium arises, highlighting the need for sustained control measures.

The sensitivity analysis underscores the critical role of parameters such as the transmission probabilities ( $\beta_{ah}$ , and  $\beta_h$ ), awareness level ( $\theta$ ), and isolation rate ( $q$ ). The findings reveal that higher public vigilance and effective isolation measures can significantly lower the number of exposed and infected individuals, thereby reducing the spread of the virus. Additionally, the results demonstrate that targeting these sensitive parameters can have a substantial impact on reducing the overall disease burden, making these measures pivotal in epidemic control strategies.

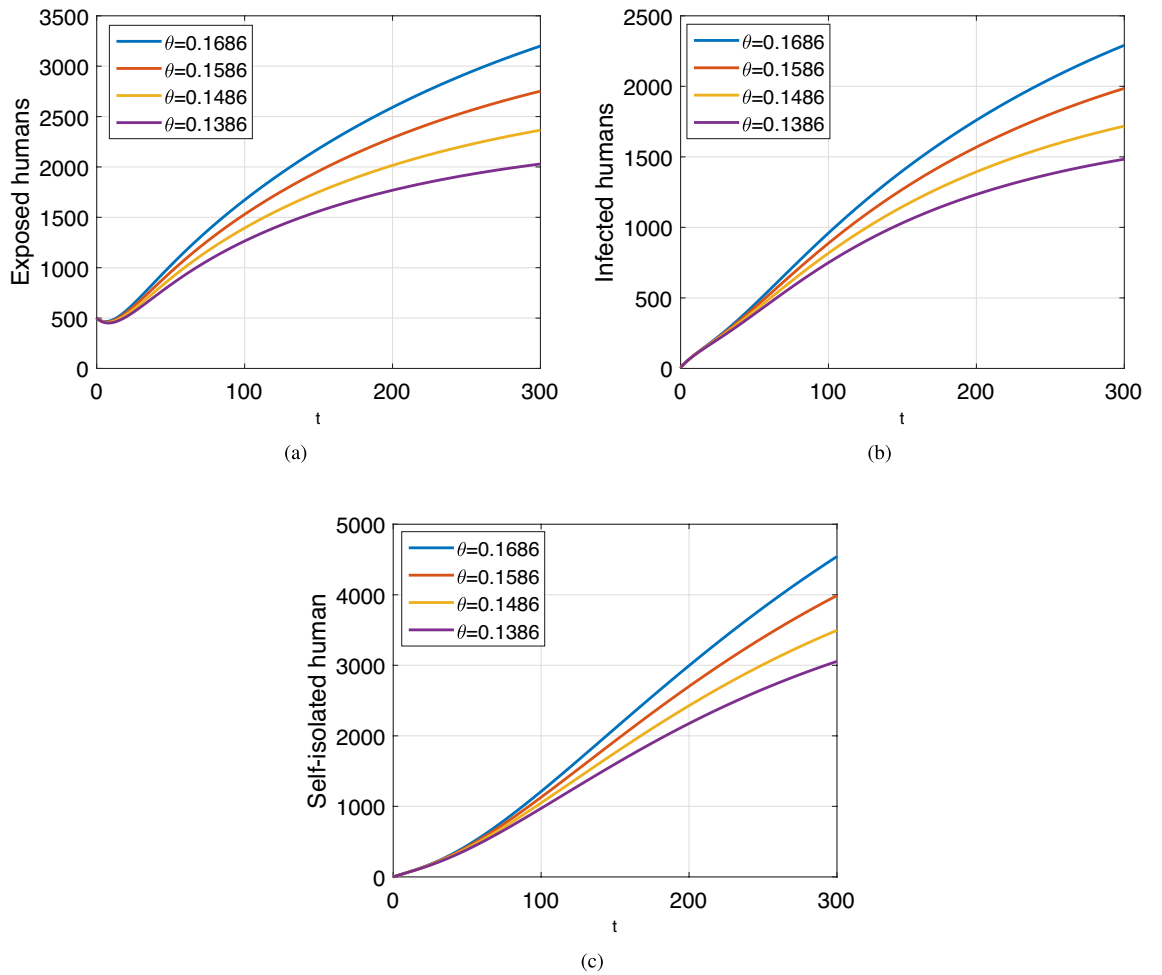


**Fig. 9.** The plot describes the dynamics of the exposed, infected, and self-isolated human individuals with different values of  $\theta$ . Subfigures (a–c) indicate the exposed, infected, and self-isolated people.

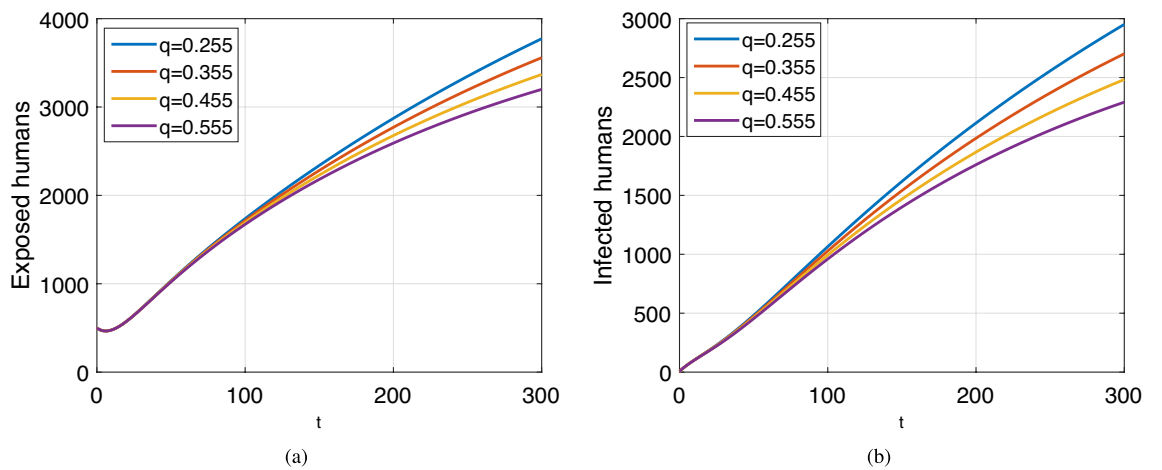


**Fig. 10.** The plot describes the dynamics of the exposed and infected human individuals for different values of  $q$ . Subfigures (a) and (b) show the temporal evolution of the exposed and infected individuals, respectively.

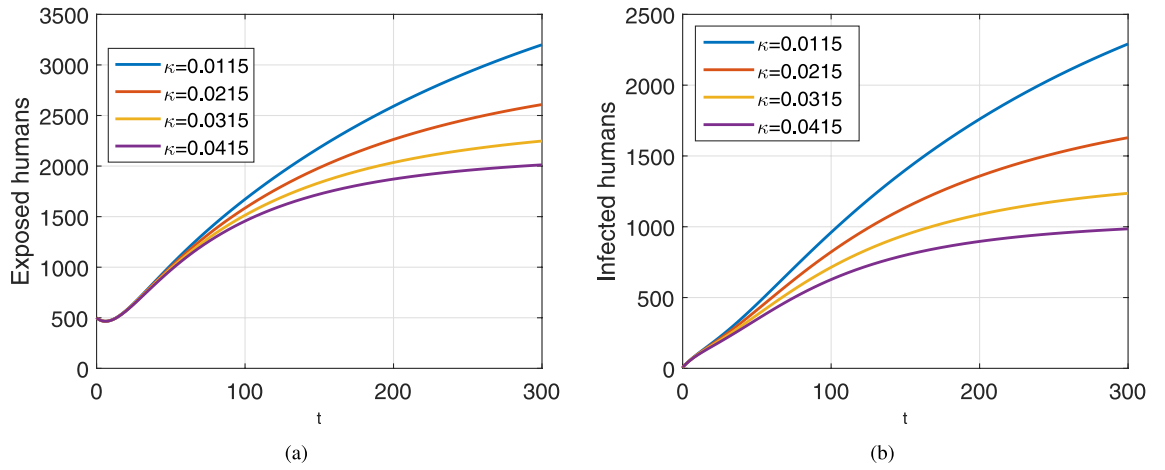


**Fig. 11.** The plot describes the dynamics of the exposed and infected human individuals with different values of  $\kappa$ . Subfigures (a) and (b) indicate the exposed and the infected individuals, respectively.

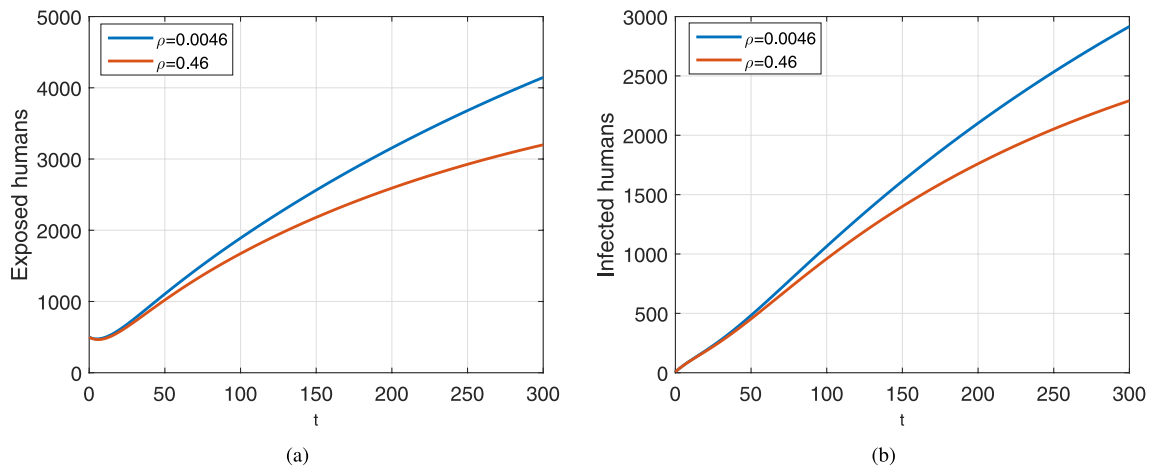


**Fig. 12.** The plot describes the dynamics of the exposed and infected human individuals with different values of  $\rho$ . Subfigures (a) and (b) indicate the exposed and the infected individuals, respectively.

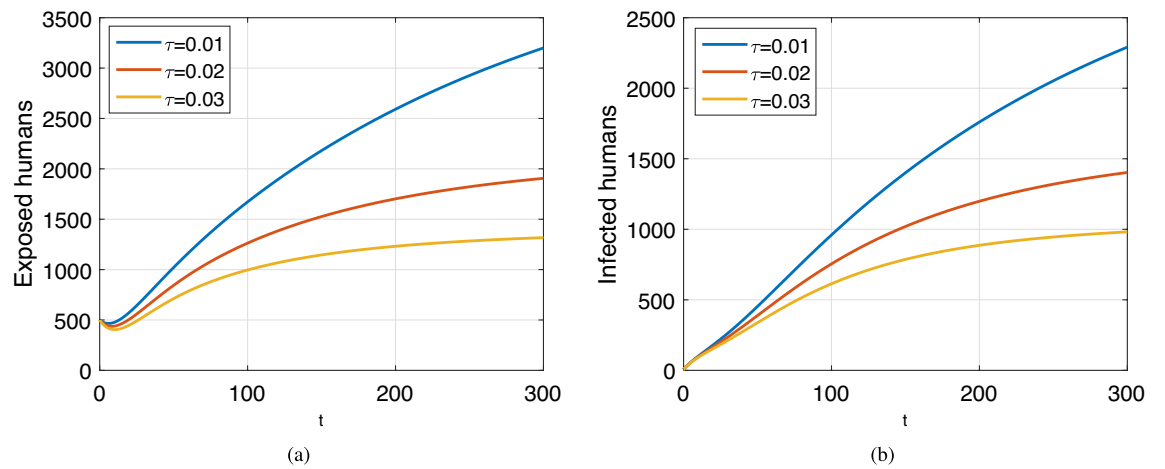


**Fig. 13.** The plot describes the dynamics of the exposed and infected human individuals with different values of  $\tau$ . Subfigures (a) and (b) indicate the exposed and the infected individuals, respectively.

The numerical simulations further illustrate how varying levels of public compliance with self-isolation and awareness campaigns can alter the course of an epidemic. Even partial compliance with these interventions can substantially mitigate the spread, emphasizing the value of community engagement in public health efforts.

Public health interventions like isolation and awareness programs must address stigmatization risks and socioeconomic barriers to compliance, particularly for high-risk groups. Ethical implementation through financial support, culturally sensitive messaging, and anonymized testing can enhance effectiveness while minimizing harm. Our findings on partial compliance underscore the need for inclusive strategies that balance public health goals with equity.

In summary, the study offers a robust framework for understanding the dynamics of mpox transmission and highlights the importance of tailored interventions. The insights derived from this research can inform policymakers in designing more effective response strategies to combat current and future mpox outbreaks. The findings, supported by real-world data and rigorous analysis, make a significant contribution to the field of infectious disease modeling and can serve as a valuable reference for public health authorities aiming to minimize the impact of mpox.

We will extend this work by incorporating stochastic elements to capture random events and uncertainties in real-world disease spread. Further, an age-structure analysis of the model will provide more age-specific transmission patterns and generate targeted recommendations for different age groups. Moreover, real-time feedback mechanisms, including adaptive testing protocols, isolation measures, and mobility restrictions, will be integrated to evaluate dynamic intervention effectiveness.

## Data availability

Centers for Disease Control and Prevention (CDC). Mpox, u.s. case trends: Clade ii mpox. <https://www.cdc.gov/v/mplex/data-research/cases/index.html>. Accessed on September 20, 2024.

Received: 4 April 2025; Accepted: 7 July 2025

Published online: 26 July 2025

## References

1. World health organization (WHO). *mpox fact sheet*. <https://www.who.int/news-room/fact-sheets/detail/mpox>. Accessed on September 20, (2024).
2. Mpox (mpox)-cdc, 2023. <https://www.cdc.gov/poxvirus/mpox/if-sick/transmission.html>. Accessed on August 08, (2024).
3. Africa cdc, center for disease control and prevention, Africa cdc epidemic intelligence weekly report. <https://africacdc.org/download/africa-cdc-weekly-event-based-surveillance-report-august-2024/> Accessed on August 17, (2024).
4. Who recommended the new name-mpox. <https://news.un.org/en/story/2022/11/1131082>. Accessed on August 18, (2024).
5. Bulletin of the atomic scientist (bas). *A new mpox variant is taking off in Africa*. The who plan for stopping it isn't realistic.
6. Simar Bajaj. *What you need to know about the history of monkeypox*. *Smithson Mag.* (2002). <https://www.smithsonianmag.com/history/what-you-need-to-know-about-the-history-of-monkeypox-180980301/> Accessed on August 17, 2024.
7. Morris, S. et al. A systematic review on human monkeypox virus disease and infection in pregnancy. *Journal of Pure Applied Microbiology*. **17** (2023).
8. Grant, R., Nguyen, L. B. L. & Breban, R. Modelling human-to-human transmission of mpox. *Bull. World Health Organ* **98**, 634–640 (2020).
9. Usman, S. et al. Modeling the transmission dynamics of the monkeypox virus infection with treatment and vaccination interventions. *J. Appl. Math. Phys.* **5**, 2335 (2017).
10. Bhunu, C. & Mushayabasa, S. Modelling the transmission dynamics of pox-like infections. *IAENG Int. J.* **41**, 141–149 (2011).
11. Somma, S. A. & Akinwande, N. I. Sensitivity analysis for the mathematical modelling of mpox virus incorporating quarantine and public enlightenment campaign. *FULafia J. Sci. Technol.* **6**, 54–61 (2020).
12. Madubueze, C. E., Onwubuya, I. O., Nkem, G. N. & Chazuka, Z. The transmission dynamics of the monkeypox virus in the presence of environmental transmission. *Front. Appl. Math. Stat.* **8**, 1061546 (2022).
13. Fernandes, G. & Maldonado, V. Behavioral aspects and the transmission of monkeypox: A novel approach to determine the probability of transmission for sexually transmissible diseases. *Infect. Disease Modell.* **8**, 842–854 (2023).
14. Brand, S. P. et al. The role of vaccination and public awareness in forecasts of mpox incidence in the united kingdom. *Nat. Commun.* **14**, 4100 (2023).
15. Camponovo, F., Ockenhouse, C. F., Lee, C. & Penny, M. A. Mass campaigns combining antimalarial drugs and anti-infective vaccines as seasonal interventions for malaria control, elimination and prevention of resurgence: a modelling study. *BMC Infect. Diseases* **19**, 1–15 (2019).
16. Egonmwan, A. & Okuonghae, D. Mathematical analysis of a tuberculosis model with imperfect vaccine. *Int. J. Biomath.* **12**, 1950073 (2019).
17. Zhao, S. et al. Preliminary estimation of the basic reproduction number of novel coronavirus (2019-ncov) in china, from 2019 to 2020: A data-driven analysis in the early phase of the outbreak. *Int. J. Infect. Diseases* **92**, 214–217 (2020).
18. McNeill, W. H. *Plagues and Peoples* 216 (Anchor press, Garden city, 1976).
19. Manivel, M., Venkatesh, A. & Kumawat, S. A comprehensive study of monkeypox disease through fractional mathematical modeling. *Math. Modell. Numer. Simul. Appl.* **5**, 65–96 (2025).
20. Collins, O. C. & Duffy, K. J. Dynamics and control of mpox disease using two modelling approaches. *Model. Earth Syst. Environ.* **10**, 1657–1669 (2024).
21. Frank, T. D. Mathematical analysis of four fundamental epidemiological models for monkeypox disease outbreaks: On the pivotal role of human-animal order parameters-in memory of hermann haken. *Mathematics* **12**, 3215 (2024).
22. Gümüş, M. & Türk, K. Global analysis of a monkeypox virus model considering government interventions. *Physica Scripta* **100**, 045216 (2025).
23. Omame, A. et al. Dynamics of mpox in an HIV endemic community: A mathematical modelling approach. *Math. Biosci. Eng.* **22**, 225–259 (2025).
24. Deng, Q. et al. Uncovering the impact of infection routes on within-host mpox dynamics: Insights from a mathematical modeling study. *PLOS Computat. Biol.* **21**, e1013073 (2025).
25. Should you worry about rising mpox cases?. <https://www.verywellhealth.com/united-states-mpox-case-increase-2024-8627960>. Accessed on October 20, (2024).
26. Van den Driessche, P. & Watmough, J. Reproduction numbers and sub-threshold endemic equilibria for compartmental models of disease transmission. *Math. Biosci.* **180**, 29–48 (2002).

27. LaSalle, J. P. Stability theory and invariance principles. In *Dynamical Systems*, 211–222 (Elsevier, 1976).
28. Yadav, R. et al. Mpox 2022 to 2025 update: A comprehensive review on its complications, transmission, diagnosis, and treatment. *Viruses* **17**, 753 (2025).
29. UK Health Security Agency. Mpox outbreak: epidemiological overview, 5 June 2025. Technical report GOV-18851, UK Health Security Agency, England, UK (2025). Updated 5 June 2025; current through 31 May 2025.
30. Constantino, A. K. Health officials confirm first U.S. case of monkeypox virus this year in massachusetts (2022). Archived June 5, 2022. Retrieved July 16, 2022.
31. Centers for Disease Control and Prevention. 2022 mpox outbreak global map (2024). Retrieved August 22, 2024.
32. Kimball, S. Texas reports what may be the first U.S. death from monkeypox (2022). Archived August 31, 2022. Retrieved August 31, 2022.
33. Centers for Disease Control and Prevention (CDC). Mpox, U.S. case trends: Clade ii mpox. <https://www.cdc.gov/mpox/data-research/cases/index.html>. Accessed on September 20, 2024.
34. Centers for Disease Control and Prevention (CDC). Center for disease control and prevention (cdc). [https://www.cdc.gov/mpox/data-research/cases/?CDC\\_AAref\\_Val=https://www.cdc.gov/poxvirus/mpox/response/2022/mpx-trends.html](https://www.cdc.gov/mpox/data-research/cases/?CDC_AAref_Val=https://www.cdc.gov/poxvirus/mpox/response/2022/mpx-trends.html). Accessed on March 20, 2024.
35. American life expectancy is now at its lowest in nearly two decades. <https://www.gpb.org/news/shots-health-news/2022/12/22/american-life-expectancy-now-at-its-lowest-in-nearly-two-decades>. Accessed on March 10, 2023
36. Chitnis, N., Hyman, J. M. & Cushing, J. M. Determining important parameters in the spread of malaria through the sensitivity analysis of a mathematical model. *Bullet. Math. Biol.* **70**, 1272–1296 (2008).

## Acknowledgements

The authors are thankful to the Deanship of Research and Graduate Studies, King Khalid University, Abha, Saudi Arabia, for financially supporting this work through the Large Research Group Project under Grant no. R. G. P. 2/409/46.

## Author contributions

Akindele Akano Onifade: Formulation, Writing, Investigation, Formal analysis, Methodology, Visualization, Review & editing. Oluwaseun Adenike Akindele: Validation, Methodology, Resources, Visualization. Irfan Ahmad: Methodology, Writing, Formal analysis, Investigation. Muhammad Altaf Khan: Formulation, Writing, Investigation, Formal analysis, Methodology, Visualization, Software, Review & editing, Supervision. Nurulfiza Mat Isa: Writing, Investigation, Methodology, Visualization, Review & editing, Supervision. Ebraheem Alzahrani: Formal analysis, Methodology, Visualization, Review & editing. All authors reviewed the manuscript and approved the final version for submission.

## Declarations

### Competing interests

The authors are declared that they no potential conflict of interest regarding the publication of this work.

### Additional information

**Correspondence** and requests for materials should be addressed to M.A.K.

**Reprints and permissions information** is available at [www.nature.com/reprints](http://www.nature.com/reprints).

**Publisher's note** Springer Nature remains neutral with regard to jurisdictional claims in published maps and institutional affiliations.

**Open Access** This article is licensed under a Creative Commons Attribution-NonCommercial-NoDerivatives 4.0 International License, which permits any non-commercial use, sharing, distribution and reproduction in any medium or format, as long as you give appropriate credit to the original author(s) and the source, provide a link to the Creative Commons licence, and indicate if you modified the licensed material. You do not have permission under this licence to share adapted material derived from this article or parts of it. The images or other third party material in this article are included in the article's Creative Commons licence, unless indicated otherwise in a credit line to the material. If material is not included in the article's Creative Commons licence and your intended use is not permitted by statutory regulation or exceeds the permitted use, you will need to obtain permission directly from the copyright holder. To view a copy of this licence, visit <http://creativecommons.org/licenses/by-nc-nd/4.0/>.

© The Author(s) 2025